Master's thesis

NTNU
Norwegian University of Science and Technology
Faculty of Medicine and Health Sciences
Department of Clinical and Molecular Medicine

Johan E. Guthormsen

Overexpression of miR-210 rescues human cardiomyocytes from doxorubicin-induced stress

Master's thesis in Pharmacy
Supervisor: Morten Høydal
Co-supervisor: Gurdeep Marwarha
May 2024

NTNU
Norwegian University of
Science and Technology

Johan E. Guthormsen

Overexpression of miR-210 rescues human cardiomyocytes from doxorubicin-induced stress

Master's thesis in Pharmacy
Supervisor: Morten Høydal
Co-supervisor: Gurdeep Marwarha
May 2024

Norwegian University of Science and Technology
Faculty of Medicine and Health Sciences
Department of Clinical and Molecular Medicine

NTNU
Norwegian University of
Science and Technology

Abstract

Background: Diagnostic and treatment-related improvements in cancer management have led to an increase in patients surviving their malignant diseases. This increase has been accompanied by a rise in survivors experiencing treatment-induced health issues. Chemotherapy-induced cardiac damage constitutes one such problem, and doxorubicin is one of the most notorious cardiotoxic anticancer drugs. This drug is widely used for cancers such as breast cancer, lymphoma, and childhood cancers. Its usage is associated with cumulative dose-dependent cardiotoxicity, leading to cardiomyopathy and, eventually, congestive heart failure. Moreover, since their discovery just over 30 years ago, microRNAs have been described as key players in the regulation of gene networks and in modifying complex biological processes. One such microRNA, miR-210, promotes the survival of numerous cell types under hypoxic conditions. Current prevention strategies of managing doxorubicin-cardiac damage are insufficient, and miR-210 have shown promising results in both *in vitro* and *in vivo* studies of ischemic cardiac disease. As such, this thesis studies the effects of miR-210 on cell death, cell viability, and apoptosis in human AC-16 cardiomyocytes. In addition, the Akt-GSK-3β signaling pathway was explored in relation to apoptosis.

Methods: miR-210 was upregulated or downregulated in AC-16 cardiomyocytes using transient expression or decoy/inhibitory transfection vectors before being subject to 5 μM doxorubicin treatment for 24 hours. General cell death was determined using a lactate dehydrogenase (LDH)-release assay, while cell viability was examined using an MTT assay. Apoptotic cell death was determined by a caspase-3 activity assay, and the Akt-GSK-3β signaling pathway was explored using a sandwich enzyme-linked immunosorbent assay (ELISA) approach. Additionally, an *in silico* search was performed to identify potential miR-210 target genes serving as a link to the Akt-GSK-3β signaling pathway.

Results: Upregulation of miR-210 in AC-16 cardiomyocytes exposed to 24 hours doxorubicin treatment caused a significant reduction in general cell death ($p < 0.001$), a significant increase in cell viability ($p < 0.05$), and a significant reduction in apoptotic cell death ($p < 0.0001$). Downregulation of miR-210 in AC-16 cardiomyocytes exposed to the same conditions resulted in a significant increase in general cell death ($p < 0.0001$) and in apoptotic cell death ($p < 0.0001$), while no effect on cell viability was observed. An increase in both p-Ser9 GSK-3β ($p < 0.0001$) and p-Ser473 Akt ($p < 0.01$) was observed in the miR-210-upregulated group, while a decrease in p-Ser473 Akt ($p < 0.5$) but no difference in p-Ser9 GSK-3β was observed in the miR-210-downregulated group. *KMT2D*, *RAP2B*, *EFNA3*, *E2F3*, *ATG7*, *BDNF*, and *HIF3A* were identified as the potential miR-210 target genes having an experimentally determined link to Akt.

Conclusion: miR-210 exerts cytoprotective effects in AC-16 cardiomyocytes exposed to 24 hours of doxorubicin treatment by reducing cell death, increasing cell viability, and inhibiting apoptosis through modulation of the Akt-GSK-3β signaling pathway. Thus, this thesis suggests a novel role of miR-210 in mitigating DOX-induced cardiomyocyte death, highlighting its potential as a therapeutic target.

Sammendrag

Bakgrunn: Fremskritt i tidlig diagnostikk og behandling av kreftsykdommer har ført til en økning i antall pasienter som overlever kreft. Denne økningen har samtidig ført til at stadig flere pasienter lever med helseproblemer forårsaket av selve behandlingen. Kjemoterapi-indusert hjertesykdom utgjør et slikt problem, og doxorubicin er et av legemidlene som er mest beryktet for å forårsake hjertetoksisitet. Dette legemidlet er mye brukt i behandling av kreftsykdommer som brystkreft, lymfom og kreft hos barn. Bruken er forbundet med akkumulativ doseavhengig hjertetoksisitet, som fører til kardiomyopati, en tilstand som kan utvikle seg til hjertesvikt. MikroRNA, oppdaget for drøyt 30 år siden, spiller en avgjørende rolle i reguleringen av gennettverk og modifiseringen av komplekse biologiske prosesser. Et slikt mikroRNA, miR-210, promoterer overlevelsen til en rekke celletyper under hypoksi. Tilgjengelige strategier for å håndtere doxorubicin-indusert hjertesykdom er i dag utilstrekkelige, og miR-210 har vist lovende resultater i både *in vitro*- og *in vivo*-studier av iskemisk hjertesykdom. Dermed var formålet med denne oppgaven å studere effektene av miR-210 på celledød, celleviabilitet og apoptose i humane AC-16 hjertemuskelceller. I tillegg utforskes Akt-GSK-3β-signalveien i forbindelse med apoptose.

Metoder: miR-210 ble oppregulert og nedregulert i AC-16 hjertemuskelceller ved bruk av midlertidige overuttrykks- eller inhibitoriske transfeksjonsvektorer før cellene ble behandlet med 5 μM doxorubicin i 24 timer. Generell celledød ble studert gjennom en laktatdehydrogenase (LDH)-release assay, mens celleviabilitet ble studert gjennom en MTT-assay. Apoptotisk celledød ble studert ved hjelp av en caspase-3 activity assay, og Akt-GSK-3β-signalveien ble utforsket ved bruk av en sandwich enzyme-linked immunosorbent assay (ELISA)-tilnærming. I tillegg ble det utført et *in silico*-søk for å identifisere mulige miR-210-målgener som kunne fungere som en forbindelse til Akt-GSK-3β-signalveien.

Resultater: Oppregulering av miR-210 i AC-16 hjertemuskelceller eksponert for 24 timer doxorubcinbehandling forårsaket en signifikant reduksjon i generell celledød ($p < 0,001$), en signifikant økning i celleviabilitet ($p < 0,05$) og en signifikant reduksjon i apoptotisk celledød ($p < 0,0001$). Nedregulering av miR-210 i AC-16 hjertemuskelceller eksponert for de samme eksperimentelle betingelsene resulterte i en signifikant økning i generell celledød ($p < 0,0001$) og i apoptotisk celledød ($p < 0,0001$), men ingen effekt på celleviabiliteten ble observert. En økning i både p-Ser9 GSK-3β ($p < 0,0001$) og p-Ser473 Akt ($p < 0,01$) ble observert i gruppen hvor miR-210 var oppregulert, mens en nedgang i p-Ser473 Akt ($p < 0,5$) ble observert i gruppen hvor miR-210 var nedregulert. Ingen endring i p-Ser9 GSK-3β ble observert i denne gruppen. *KMT2D*, *RAP2B*, *EFNA3*, *E2F3*, *ATG7*, *BDNF* og *HIF3A* ble identifisert som mulige målgener for miR-210 med en eksperimentelt bestemt forbindelse til Akt.

Konklusjon: miR-210 utøver cellebeskyttende effekter i AC-16 hjertemuskelceller utsatt for 24 timer med doxorubicinbehandling. Disse effektene skyldes redusert celledød, økt celleviabilitet og redusert apoptose. Reduksjonen i apoptose medieres gjennom modulering av Akt-GSK-3β-signalveien. Dermed foreslås det i denne oppgaven en ny rolle for miR-210 i å redusere doxorubicin-indusert celledød i hjertemuskelceller, og fremhever dets potensial som et terapeutisk mål.

Acknowledgements

This master's thesis was carried out at the Department of Circulation and Medical Imaging, Faculty of Medicine and Health Sciences, Norwegian University of Science and Technology (NTNU), Trondheim. My supervisor for this project has been Professor Morten Høydal, Head of the Group of Molecular and Cellular Cardiology, and my co-supervisor has been Dr. Gurdeep Marwarha.

I would like to thank my supervisor, Morten, for the opportunity to write my master's thesis in your group and for granting me invaluable experience in conducting basic research. I am also grateful for your constructive feedback and inspirational advice throughout this process. Next, I would like to thank my co-supervisor, Gurdeep, for teaching me laboratory techniques, providing me with experimental procedures, and helping me with my experiments. Your knowledge, experience, and explanations of different concepts have been invaluable to me throughout this process.

I would also like to thank the rest of the Group of Molecular and Cellular Cardiology for making me feel like a part of the team. Thank you for your willingness to share your knowledge and for offering to help me if I needed it; it is much appreciated. Penultimately, I want to thank my family for encouragement and support throughout this journey.

Finally, I would like to thank my fellow students, Mido and Mikal, for making this year an unforgettable one. The laughs, long laboratory sessions, and experiences we shared together throughout this process are something that I am truly grateful for.

Table of contents

List of figures ix
List of tables ix
Commonly used abbreviations x
1 Introduction 11
1.1 Doxorubicin-induced cardiotoxicity 11
1.2 MicroRNA-210 15
2 Aim 18
3 Materials and methods 19
3.1 Cells and subculturing 19
3.2 Transfection procedure 20
3.3 Doxorubicin treatment 22
3.4 Harvesting the cells and preparation of cell lysates 22
3.5 Bradford assay 22
3.6 MTT assay 23
3.7 Sandwich enzyme-linked immunosorbent assays (ELISAs) 23
3.7.1 Lactate dehydrogenase (LDH)-release assay 25
3.7.2 β-Actin ELISA immunoassay 26
3.7.3 GSK-3β, p-Ser9 GSK-3β, Akt, and p-Ser473 Akt ELISA immunoassays 26
3.8 Enzyme-linked miR-210 hybridization immunoassay 26
3.9 Caspase-3 activity assay 27
3.10 Bioinformatics 27
3.11 Statistical analysis 27
4 Results 28
4.1 miR-210 increases cell viability in DOX-treated AC-16 cardiomyocytes 28
4.2 miR-210 reduces cell death in DOX-treated AC-16 cardiomyocytes 29
4.3 miR-210 inhibits apoptosis in DOX-treated AC-16 cardiomyocytes 29
4.4 miR-210 inhibits DOX-induced apoptotic cell death by affecting phosphorylation status of GSK-3β 30
4.5 miR-210 affects phosphorylation status of Akt in DOX-treated AC-16 cardiomyocytes 32
4.6 Predicted miR-210 target genes and their relationship to Akt 34
5 Discussion 35
5.1 Effects of miR-210 on DOX-induced AC-16 cardiomyocyte death 35
5.2 Predicted miR-210 target genes and Akt 37
5.3 Future perspectives 39

5.4 Limitations 40
6 Conclusion 41
7 References 41

List of figures

Figure 1. Simplified overview of the intrinsic and extrinsic apoptotic pathways activated by DOX 13
Figure 2. miRNA processing 16
Figure 3. Subculturing procedure 20
Figure 4. Schematic representation of the experimental paradigm 21
Figure 5. Basic overview of Sandwich ELISA 25
Figure 6. miR-210 increases cell viability in DOX-treated AC-16 cardiomyocytes 28
Figure 7. Overexpression and downregulation of miR-210 affect cell death in DOX-treated AC-16 cardiomyocytes 29
Figure 8. miR-210 reduces DOX-induced apoptotic cell death in AC-16 cardiomyocytes. 30
Figure 9. miR-210 overexpression increases phosphorylation at serine 9 residue (Ser9) of glycogen synthase kinase-3β (GSK-3β) in DOX-treated AC-16 cardiomyocytes 31
Figure 10. miR-210 affects phosphorylation of Akt at serine 473 (Ser473) in DOX-treated AC-16 cardiomyocytes 33
Figure 11. Predicted miR-210 target genes and their relationship to Akt 34
Figure 12. Proposed protective mechanism of upregulation of miR-210 in DOX-treated AC-16 cardiomyocytes 39

List of tables

Table 1. List of antibodies and antibody-blocking peptides utilised in this study 24

Commonly used abbreviations

AP	Alkaline phosphatase
ATG7	Autophagy related 7
ATP	Adenosine triphosphate
BCL-2	B-cell lymphoma-2
BDNF	Brain derived neurotrophic factor
BH	BCL-2 homology
DOX	Doxorubicin
DNA	Deoxyribonucleic acid
E2F3	E2F transcription factor 3
EFNA3	Ephrin A3
ELISA	Enzyme-linked immunosorbent assay
EV	Empty vector
GSK-3β	Glycogen synthase kinase-3β
HIF1α	Hypoxia-inducible factor 1α
HIF3A	Hypoxia inducible factor 3 subunit alpha
KD	miR-210 knockdown
KMT2D	Lysine methyltransferase 2D
LDH	Lactate dehydrogenase
mRNA	Messenger RNA
miRNA	MicroRNA
miR-210	MicroRNA-210-3p
MTT	3-(4,5-dimethylthiazol-2-yl)-2,5-diphenyl-2H-tetrazolium bromide
OE	miR-210 overexpression
PI3K	Phosphoinositide 3-kinase
PNPP	P-nitrophenyl phosphate, disodium salt
p-Ser473 Akt	Phosphorylated Akt at serine residue 473
p-Ser9 GSK-3β	Phosphorylated GSK-3β at serine residue 9
RAP2B	RAP2B, member of RAS oncogene family
RNA	Ribonucleic acid
ROS	Reactive oxygen species
TET2	Ten-eleven translocation 2

1 Introduction

Doxorubicin (DOX) is an anthracycline chemotherapeutic agent commonly used in the treatment of cancers such as breast cancer, lymphoma, and childhood cancers. Due to improvements in treatment and early diagnosis, the overall survival rate of multiple cancer types has increased in recent years. Consequently, attention has expanded beyond cancer remission to also encompass quality of life in long-term survivorship. A major drawback with DOX treatment is its inherent dose-dependent cardiotoxicity, leading to clinical decompensation in 2-4%, sub-clinical structural change in 9-11%, and arrhythmia in > 12% of treated patients (1). This not only severely limits the clinical utility of DOX but also gives rise to a novel cohort of patients requiring treatment for cardiac-related issues. Hence, intense research efforts have gone into developing therapeutic interventions for managing these issues, employing both pharmacological and non-pharmacological strategies. Despite this, many of the interventions have not translated from preclinical and clinical studies into clinical practice. As such, there exists an unmet clinical need for effective strategies to reduce DOX-induced cardiotoxicity.

1.1 Doxorubicin-induced cardiotoxicity

Since receiving approval by the Food and Drug Administration (FDA) in 1974, DOX, either alone or in combination with other chemotherapeutic agents, has been extensively utilized as a first-line treatment for a variety of solid tumors and hematological cancers (2). It was discovered at Farmitalia in the late 1960s, where it was isolated from a mutated strain of the bacterium *S. peucetius* var. *caesius* (3). DOX is a member of the anthracycline class of cytotoxic antibiotics, which act by intercalating into DNA, inhibiting topoisomerase enzymes, disrupting mitochondrial function, and increasing free-radical production and oxidative damage (4). In addition to the dose-dependent cardiotoxicity, anthracycline use is also associated with numerous other adverse effects, ranging from generally acute and chemo-related phenomena, such as nausea, vomiting, mucositis, and bone marrow suppression, to long-term adverse effects, as treatment-related malignancies and gonadotoxicity (3).

Still, it is the cardiotoxic effects that constitute the most serious events and impose a limitation on its clinical usefulness. The use of DOX may lead to progressive secondary cardiomyopathy, which is defined as a disease of the heart muscle resulting from an extravascular cause (5). Eventually, this condition may evolve into congestive heart failure, which has a poor prognosis (6). However, patients without additional risk factors typically tolerate cumulative DOX doses of up to 300 mg/m^2 moderately well, with a reported heart failure rate of less than 2% (7). Exceeding this dosage threshold, however, markedly increases the rates of cardiotoxicity, which rise exponentially (8). Moreover, numerous risk factors have been associated with increased sensitivity to developing DOX-induced cardiotoxicity; these include age, genetic predisposition, co-existing cardiovascular diseases, concurrent mediastinal radiation therapy, and combination with other chemotherapeutic agents (8). Especially, elderly individuals (> 65 years of age) and children may be susceptible to developing clinical symptoms of cardiomyopathy at lower cumulative doses. In patients with childhood acute lymphoblastic leukemia treated with DOX, survivors showed persistent cardiac abnormalities such as reduced left ventricular contractility and abnormal left ventricular structure, which progressively worsened over time (9). This occurred even at a

cumulative dose of less than 300 mg/m^2 (9). Due to these deleterious effects, it is advised that the lifetime cumulative dose of DOX not exceed 400-450 mg/m^2 (10).

Mechanistically, DOX-induced cardiotoxicity is an intricate process involving free radical-induced oxidative stress, dysregulation of calcium handling, adrenergic dysfunction, and selective inhibition of cardiomyocyte-specific gene expression (11). Given its especially high mitochondrial density/volume compared to other organs, the heart is particularly sensitive to the oxidative damage caused by DOX, as mitochondria are both major sources and targets of reactive oxygen species (ROS) (12). Through a process termed redox cycling, which involves the reduction and re-oxidization of DOX mediated by cellular oxidoreductase enzymes, ROS such as the superoxide anion radical (O_2^-) and hydrogen peroxide (H_2O_2) are generated (10, 13). These molecules can further be converted to the highly reactive and toxic hydroxyl radicals (·OH), which, upon oxidation of cellular components, result in severe cellular damage (10). Moreover, DOX also causes oxidative stress through other mechanisms, such as iron complexation and uncoupling of the electron transport chain in the mitochondria, and by disrupting antioxidant defense systems (14). Additionally, in comparison with other tissues, the heart has relatively low levels of antioxidant-producing enzymes, such as peroxidase, superoxide dismutase, and catalase, making it even more vulnerable to DOX-induced oxidative stress (15, 16). In cardiomyocytes, DOX targets the enzyme topoisomerase-IIβ, and the resulting topoisomerase-IIβ-DOX-DNA complex can cause DNA double-strand breaks (17). Most of these cellular events trigger signaling pathways that culminate in cardiomyocyte death, which is a major contributor to DOX-induced cardiomyopathy (11).

The most studied cell death pathway in DOX-induced cardiomyocyte death is apoptosis (18). Apoptosis itself can be subdivided into intrinsic and extrinsic types, which differ in how the initiating signals are perceived and managed by the cell. Intrinsic apoptosis can be triggered by numerous molecular events, including growth factor withdrawal, mitochondrial impairment, DNA damage, and cytotoxic chemicals (19, 20). When the intrinsic pathway is activated, the B-cell lymphoma-2 (BCL-2) family of proteins serves as the main upstream regulators. This family is characterized by one to four BCL-2 homology (BH) domains and includes both pro-apoptotic and anti-apoptotic members (19). These domains are highly conserved across the family, with most members also possessing a carboxy-terminal hydrophobic domain that facilitates their association with intracellular membranes (21). The interaction between pro-apoptotic and anti-apoptotic members, mediated by these domains, plays a crucial role in either promoting or preventing apoptosis (19, 21). Specifically, the BH3-only BCL-2 proteins, such as Bcl-2-interacting mediator of cell death, BH3 interacting-domain death agonist, Bcl-2-associated death promoter, NOXA, and p53 upregulated modulator of apoptosis, promote apoptosis by activating Bcl-2-associated X protein and Bcl-2 homologous antagonist/killer. They also promote apoptosis by inhibiting anti-apoptotic proteins like BCL-2, B-cell lymphoma-extra large, Myeloid cell leukemia sequence 1, and BCL2-like 2 protein. These interactions are mediated through their BH3 domains and lead to the formation of oligomeric pores in the outer mitochondrial membrane (19, 22). This process is known as mitochondrial outer membrane permeabilization and causes the release of cytochrome c, which subsequently binds to apoptotic protease activating factor-1 monomers, culminating in the assembly of the heptameric apoptosome (23). In addition to cytochrome c and apoptotic protease activating factor-1, the apoptosome also incorporates procaspase-9, a member of the caspase family. Caspases are cysteine proteases best known for being the effectors of the regulated cell death pathways apoptosis and pyroptosis (23, 24). Formation of the apoptosome initiates the cleavage

and activation of procaspase-9 into caspase-9, which in turn activates downstream executioner caspases like caspase-3 and caspase-7, leading to the cleavage of numerous cellular proteins and ultimately promoting cellular destruction (19, 23, 24). The intrinsic apoptotic cascade is triggered by DOX through various mechanisms such as the upregulation of p53, the downregulation of GATA-binding protein 4, and the inactivation of the phosphoinositide 3-kinase (PI3K)-Akt pro-survival pathway (18).

Extrinsic apoptosis, on the other hand, can be initiated via death receptors belonging to the tumor necrosis factor receptor superfamily (25). Binding of death ligands such as Fas Ligand or tumor necrosis factor-α to their respective plasma membrane death receptors triggers the recruitment of cytosolic death domain proteins (18). These adaptor proteins, Fas-associated death domain or TNFR-associated death domain, then interact with initiator procaspases-8 or -10, leading in turn to their autoactivation (18, 25, 26). Furthermore, caspase-8 and/or caspase-10 activates downstream executioner caspases like caspase-3 and caspase-7 (27). The extrinsic apoptotic cascade is triggered by DOX via the upregulation of the transcription factors nuclear factor of activated T-cells 4 and nuclear factor-kappa B, in addition to the upregulation of death receptors (18). A simplified overview of DOX-induced apoptotic cell death is provided in Fig. 1.

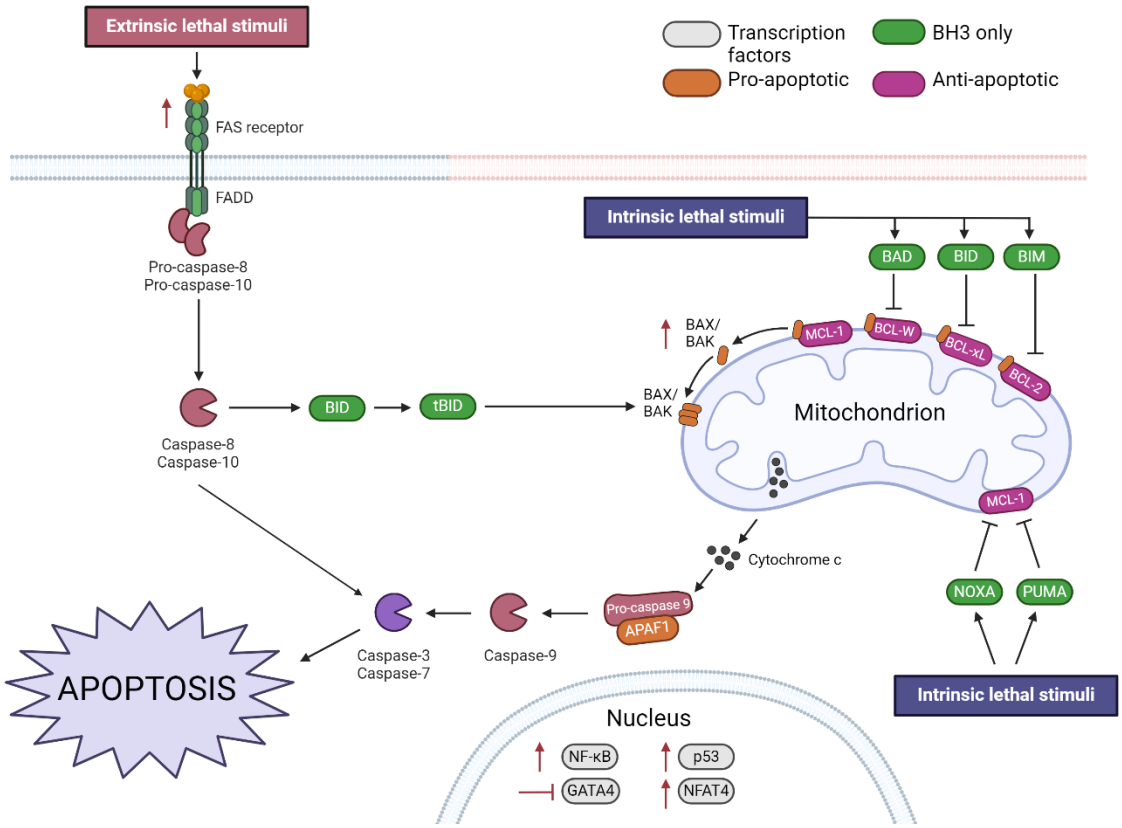

Figure 1. Simplified overview of the intrinsic and extrinsic apoptotic pathways activated by DOX. *Treatment with DOX causes increased oxidative stress, mitochondrial damage, DNA double-strand breaks, and calcium dysregulation, culminating in the activation of apoptosis. This apoptotic response is further amplified by DOX-induced upregulation of p53 and BAK/BAX, along with the downregulation of GATA4, which collectively enhance the intrinsic apoptotic cascade. Additionally, the extrinsic apoptotic cascade is activated through DOX-induced upregulation of NFAT4, NF-κB, and death receptors such as the FAS receptor. Black arrows indicate positive regulation, black inhibitory lines indicate negative regulation, red arrows indicate upregulation by DOX, and red inhibitory lines indicate downregulation by DOX. Abbreviations: APAF1: apoptotic*

protease activating factor-1; BAD: Bcl-2-associated death promoter; BAK: Bcl-2 homologous antagonist/killer; BAX: Bcl-2-associated X protein; BCL-2: B-cell lymphoma-2; BCL-W: BCL2-like 2 protein; BCL-xL: B-cell lymphoma-extra large; BID: BH3 interacting-domain death agonist; BIM: Bcl-2-interacting mediator of cell death; FADD: Fas-associated death domain; GATA4: GATA-binding protein 4; MCL-1: Myeloid cell leukemia sequence 1; NFAT4: nuclear factor of activated T-cells 4; NF-κB: nuclear factor-kappa B; PUMA: p53 upregulated modulator of apoptosis; tBID: truncated BID. Created with BioRender.com.

In addition to apoptosis, DOX-induced cardiotoxicity also involves other regulated and unregulated cell death mechanisms (18). Autophagy, one of the mechanisms involved, plays a crucial role in cellular homeostasis through the lysosomal degradation and recycling of intracellular organelles and macromolecules (28). This catabolic process is triggered by either the activation of the AMP-activated protein kinase pathway or the inhibition of the mammalian target of rapamycin pathway (18). The process begins with the emergence of the pre-autophagosome from endoplasmic reticulum, followed by the assembly of an initiation complex comprised of Unc-51-like kinase 1, RB1-inducible coiled coil protein 1, and autophagy-related gene 13 (18). This initiation complex facilitates the nucleation and recruitment of various tethering proteins such as Beclin 1, which is phosphorylated by Unc-51-like kinase 1. This phosphorylation activates vacuolar protein sorting 34 and vacuolar protein sorting 15, which in turn recruit multiple autophagy-related gene proteins, culminating in autophagosome formation (29). Dysregulation of autophagy has been implicated in DOX-induced cardiotoxicity, with evidence suggesting that correcting this dysregulation can enhance cell viability (30, 31). In the context of DOX-induced cardiotoxicity, it has been observed that DOX impairs autophagic flux in cardiomyocytes, resulting in the accumulation of undegraded autolysosomes due to inadequate lysosome acidification (31, 32).

DOX also triggers an iron-dependent regulated cell death pathway termed ferroptosis (33). The administration of DOX leads to iron accumulation through inactivation of ferritin and the upregulation of the transferrin receptor (18). This results in a rise in intracellular free iron that interacts with DOX, causing the generation of ROS through the Fenton reaction (18). Moreover, DOX contributes to lipid peroxidation by suppressing both mitochondrial and cytosolic glutathione peroxidase 4 (18). Specifically, in the mitochondria, DOX obstructs mitochondrial ferritin and ATP-binding cassette sub-family B member 8, augmenting iron overload (18). Heart biopsy samples from patients with heart failure due to DOX-induced cardiotoxicity reveal markedly higher levels of mitochondrial iron compared to those from other heart failure patients not affected by DOX-induced cardiotoxicity nor from healthy control subjects (34). This mitochondrial iron overload may be attributed to the DOX-induced downregulation of the ATP-binding cassette sub-family B member 8 protein, a regulator of mitochondrial iron export (34). In the nucleus, the activation of nuclear factor erythroid 2-related factor leads to an increase in heme oxygenase 1 expression, which intensifies heme breakdown and consequently elevates free iron levels, promoting ferroptosis (18). Additionally, DOX and its metabolites disrupt iron homeostasis by inactivating iron regulatory proteins 1 and 2, which then bind to iron-response elements, altering the expression of genes critical for iron metabolism (35).

Another regulated cell death pathway activated by DOX is a process termed necroptosis, which is a type of regulated necrosis dependent on receptor-interacting kinase 3 (18). DOX triggers an increase in tumor necrosis factor-α, enhancing the signaling through its receptor, tumor necrosis factor receptor 1 (18). When tumor necrosis factor receptor 1 is activated, the adapter protein TNFR-associated death domain is recruited. TNFR-

associated death domain then connects with another adapter, Fas-associated death domain, which subsequently binds to procaspase-8 (36). If caspase 8 is inhibited, receptor-interacting kinase 1 combines with receptor-interacting kinase 3 to form a complex known as the necrosome. This complex serves as crucial mediator of the necroptotic signal (36). Following this, receptor-interacting kinase 3 activates the protein mixed lineage kinase domain-like protein, which disrupts the plasma membrane, leading to the release of organelles and inflammatory factors. This release initiates an immune response and ultimately results in cellular death (18, 36). The impact of dexrazoxane and necrostatin-1 on these necroptotic components in DOX-induced cardiotoxicity indicates their role in this pathway (37).

Necrosis, generally described as energy-independent, uncontrolled cell death, is characterized by the swelling of cytoplasmic organelles and early rupture of the plasma membrane (11). Increased ROS lead to mitochondrial calcium overloading, which promotes mitochondrial permeability transition pore opening. This process causes mitochondrial swelling and ATP depletion, ultimately triggering necrotic cell death (11). In the context of DOX-induced cytotoxicity, necrosis is the dominant form of cell death at higher concentrations, while apoptosis prevails at lower concentrations (38). Nevertheless, the primary focus of this thesis is connected to apoptotic cell death.

1.2 MicroRNA-210

MicroRNAs (miRNAs) constitute a class of small, non-coding RNA molecules, approximately 22 nucleotides in length, that play a pivotal role in regulating gene expression at the post-transcriptional level. They bind to complementary sequences in the 3’ untranslated region of target messenger RNAs (mRNAs), causing translational repression or mRNA degradation, thereby modulating gene expression across a broad spectrum of biological processes (39, 40).

The biogenesis of miRNAs is a multistep process that initiates with the transcription of miRNA genes by RNA polymerase II or III into primary miRNAs (pri-miRNAs). The pri-miRNA is then processed into a precursor miRNA (pre-miRNA) by the Drosha-DGCR8 complex. Then, the pre-miRNA is exported from the nucleus to the cytoplasm, where it is further processed by Dicer into a mature miRNA duplex. The mature miRNA binds to Argonaute proteins, thereby activating the RNA-induced silencing complex, guiding the complex to complementary target mRNAs (Fig. 2) (41, 42).

MiRNAs are involved in the regulation of various cellular processes, including proliferation, differentiation, development, and apoptosis. By targeting specific mRNAs for degradation or translational repression, miRNAs serve as modulators of gene expression, ensuring precise control over protein production (43). This regulatory mechanism is essential for maintaining cellular homeostasis and responding to environmental changes.

Dysregulation of miRNA expression has been linked to numerous diseases, including cancer, neurodegenerative disorders, and cardiovascular diseases (44). In cancer, for example, specific miRNAs can act as oncogenes or tumor suppressors, depending on their targets (45). Consequently, miRNAs have emerged as potential biomarkers for disease diagnosis and prognosis, as well as novel therapeutic targets (46).

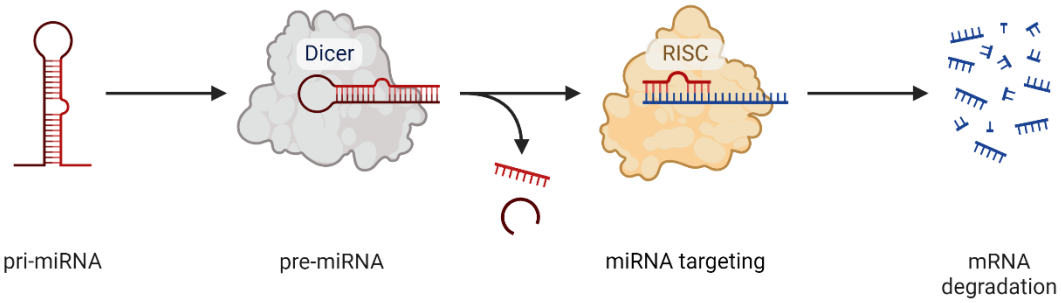

Figure 2. miRNA processing. *A transcribed pri-miRNA is processed by the Drosha-DGCR8 complex (not shown) to a pre-miRNA. Then, the pre-miRNA is cleaved by Dicer into a mature miRNA duplex. This is followed by the degradation of the most stable strand and the binding of the less stable strand to AGO and other proteins, which results in induction of the RISC and subsequent miRNA targeting. Consequently, the targeted mRNA is either degraded or translationally suppressed (not shown), which ultimately inhibits protein expression. Abbreviations: AGO: Argonaute protein; DGCR8: DiGeorge syndrome critical region gene 8; RISC: RNA-induced silencing complex; pre-miRNA: precursor-miRNA; pri-miRNA: primary-miRNA. The figure is adapted from "miRNA Processing" by BioRender.com.*

MiRNA-210 (miR-210) belongs to a subset of miRNAs termed hypoxamiRs, meaning hypoxia-induced miRNAs. It is induced in numerous ischemic diseases, including myocardial infarction (47). In a hypoxic environment, miR-210 initiates adaptive cellular responses and is implicated in processes such as angiogenesis, mitochondrial metabolism, cell cycle regulation, and apoptosis (48). Through inhibition of apoptosis and promoting angiogenesis, miR-210 is believed to protect the cardiovascular system from potentially irreversible damage upon insufficient oxygen supply (49). Under basal conditions, miR-210 appears to be transcriptionally regulated by the transcription factor activator protein 1; however, under hypoxic conditions, miR-210 is primarily induced through a hypoxia-inducible factor 1α (HIF1α) dependent mechanism (50). HIF1α-independent mechanisms, driven by the transcription factors HIF2α, nuclear factor-kappa B, and p53, are also known to play a part in the upregulation of miR-210 gene expression (49, 50).

During hypoxia, miR-210 has been shown to inhibit apoptosis in human pulmonary artery smooth muscle cells through the downregulation of E2F transcription factor 3 (E2F3) (51). Also in other cell types, such as in neural progenitor cells, miR-210 has been demonstrated to inhibit apoptosis under hypoxic conditions (52). While in AC-16 cardiomyocytes, it has been demonstrated that miR-210 attenuates the hypoxia-driven intrinsic apoptosis pathway, while significantly augmenting the reoxygenation-induced caspase-8-mediated extrinsic apoptosis pathway (53). These results show that miR-210 affects cell death by either inhibiting or promoting apoptosis, and that this effect is dependent on cellular context.

One study has shown that inhibition of glycogen synthase kinase-3β (GSK-3β) serves as the central molecular mediator for the miR-210 mitigation of intrinsic apoptosis cascade during hypoxia (54). GSK-3β is a serine/threonine protein kinase that plays a key role in transduction of regulatory and proliferative signals arising out of the cells, cytoskeletal proteins, and transcription factors (55). It is unique in that it is constitutively active in cells and its inhibition is responsible for cell signaling (56). GSK-3β is negatively

regulated by N-terminal phosphorylation of the serine 9 residue (Ser9) and positively regulated by tyrosine phosphorylation at Tyr216 (57). Moreover, stressors other than hypoxia are known to initiate the intrinsic apoptotic cascade through activation of GSK-3β, such as PI3K inhibition, DNA damage, endoplasmic reticulum stress, and mitochondrial toxins (58). In DOX-treated cardiomyocytes, pSer9 GSK-3β levels are reduced, implying increased GSK-3β activity (59).

Recently, numerous studies have explored the roles of miRNAs in DOX-induced cardiotoxicity, both *in vivo* and *in vitro* (60). As miRNAs generally have multiple target mRNAs, their potential to influence processes initiated by DOX is substantial. Moreover, several miRNAs have been shown to affect DOX-induced cardiotoxicity by targeting pathways involved in oxidative stress, apoptosis, mitochondrial function, and DNA methylation (60). While some miRNAs have been shown to exacerbate the detrimental effects, others have been demonstrated to mitigate them. Thus, understanding these diverse effects of miRNAs on DOX-induced cardiotoxicity could lead to more targeted and effective treatments for reducing chemotherapy-related cardiac damage. Furthermore, as the therapeutic potential of miR-210 in DOX-induced cardiotoxicity remains unexplored, and given its promising results in other pathological conditions, this thesis sets out to explore various facets of miR-210 biology in the context of DOX-induced cardiac cytotoxicity.

2 Aim

The main aim of this project was to explore the effects of modulating miR-210 expression levels on DOX-induced cell death in cardiomyocytes. The second aim was to investigate how miR-210 modulates cell death by evaluating central cell signaling pathways.

The main hypothesis for this study was as follows:

miR-210 overexpression attenuates DOX-induced apoptotic cell death in cardiomyocytes.

3 Materials and methods

3.1 Cells and subculturing

To study the effects of upregulating and downregulating miR-210 in cardiomyocytes exposed to DOX treatment, a cell line termed AC-16 cardiomyocytes were used. This is a cell line derived from human adult ventricular heart tissue fused with immortalized human fibroblasts. They contain the nuclear DNA and the mitochondrial DNA of the primary cardiomyocytes, are a useful *in vitro* model to study regulatory mechanisms and exploring signaling pathways, and they can be frozen and thawed repeatedly (61). However, as cell lines undergo genetic manipulations, some inherent functions and phenotypic characteristics may undergo alterations as well (62). Therefore, some limitations exist in transferring findings from cell line studies to behaviors in primary cells, e.g., AC-16 cardiomyocytes lack a functional electrophysiological machinery in contrast to primary ventricular cardiomyocytes (61).

Human AC-16 cardiomyocytes (EMD Millipore/Merck Millipore/Merk Life Sciences, Catalogue # SCC109, Darmstadt, Germany, RRID:CVCL_4U18) were cultured in Dulbecco's Modified Eagle's Medium Nutrient Mixture F-12 (DMEM/F12) (Thermo Fisher Scientific, Waltham, MA, USA), containing 12.5% fetal bovine serum (FBS) (Sigma Aldrich, Darmstadt, Germany) and 1% Antibiotic Antimycotic Solution (Sigma Aldrich, Darmstadt, Germany). DMEM with FBS and Antibiotic Antimycotic Solution is from now referred to as culture medium. AC-16 cardiomyocytes stored in liquid nitrogen were thawed and subcultured into 100-mm cell culture plates and kept in an incubator at 37 ℃ with 5% CO_2. A total of 20 cell culture plates with a confluency of ~ 80% were prepared, and 16 plates were chosen at random to be included in the experiments. The cells had a passage between 6 and 9 before the transfection step. A schematic representation of the subculturing procedure is provided in Fig. 3.

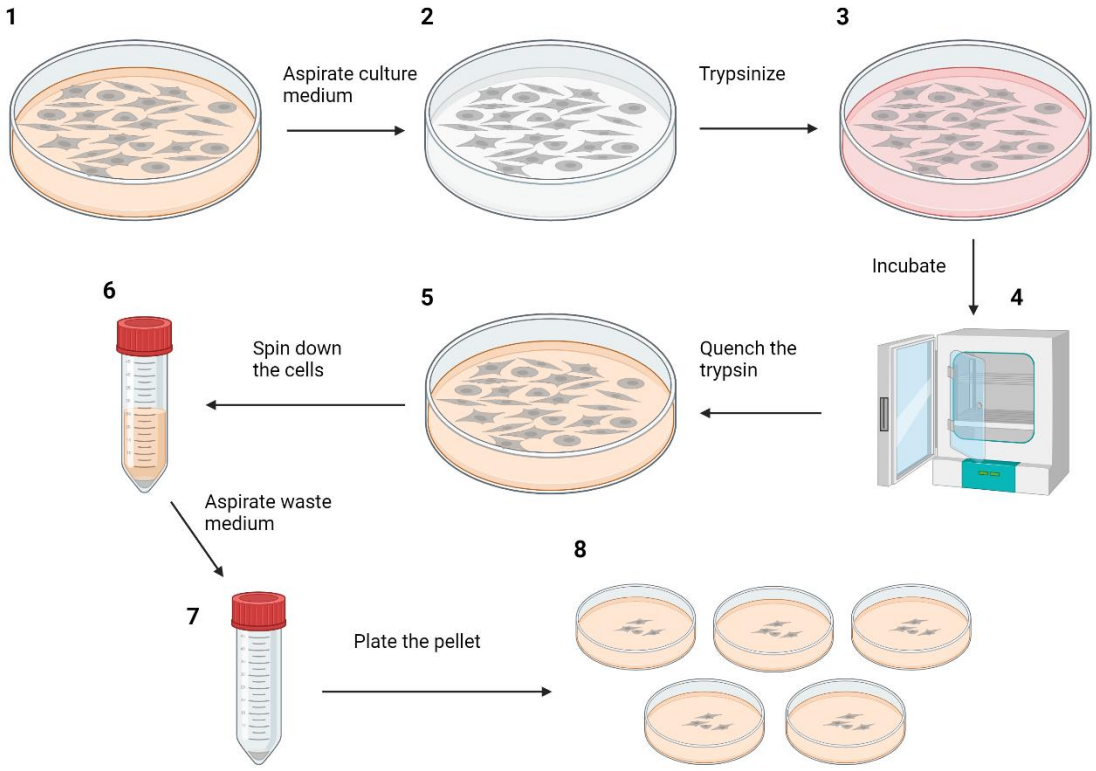

Figure 3. Subculturing procedure. *(**1**) At a confluency of ~ 80% the cells were subcultured. Firstly, the culture medium was aspirated (**2**). This was immediately followed by adding 5 mL trypsin solution (Cytiva, Marlborough, MA, USA) (**3**), so that the adherent cells would detach from the cell culture plate surface. As the optimum temperature range for trypsin is > 35 ℃, the plate was incubated (**4**) at 37 ℃ in 5% CO_2 for 3-4 mins. To ensure that the trypsin would not start to digest the cells, an equivalent amount of culture medium (5 mL) was added to quench the trypsin (**5**). Then, the cells were spun down at 500 x g for 3 min at room temperature in a centrifuge (**6**). Subsequently, the waste medium was aspirated (**7**) and the remaining pellet plated into 5 new 100-mm cell culture plates (**8**) with 10 mL culture medium in each plate. As this procedure was performed on 4 plates, this generated a total of 20 new plates, out of which 16 were chosen at random after 3-4 days of incubation (~ 80% confluency) to be part of the experiment. Created with BioRender.com.*

3.2 Transfection procedure

When the subcultured cells were ~ 80% confluent, they were transfected with the miR-210 expression vector (pEZX-MR04) (GeneCopoeia™, Rockville, MD, USA) or the miR-210-3p *decoy/inhibitor* vector (pEZX-AM01-miR-210) (GeneCopoeia™, Rockville, MD, USA). The miR-210 expression vector is from now on referred to as an overexpression (OE) vector, while the miR-210-3p *decoy/inhibitor* vector is referred to as a knockdown (KD) vector. For the control groups, an empty vector (pEZX-MR04-Scrambled) (GeneCopoeia™, Rockville, MD, USA) was used in the OE experiment, while another empty vector (pEZX-AM01-Scrambled) (GeneCopoeia™, Rockville, MD, USA) was used in the KD experiment. The experimental paradigm is outlined in Fig. 4.

A transfection mix containing 3 µg plasmid (vector), 15 µL Polyfect® transfection reagent (Qiagen, Hilden, Germany) and 150 µL plain media (DMEM without FBS and Antibiotic Antimycotic Solution) is enough to transfect one 100-mm cell culture plate

(approximately 6,000,000 cells). Therefore, a transfection mix enough for 10 plates was prepared for each group; that is, 30 µg plasmid, 150 µL transfection reagent, and 1.5 mL plain media. Firstly, the plasmid and the transfection reagent were mixed in a 1.5-mL tube, and the tube was turned upside down a few times to mix them thoroughly. Thereafter, plain media was added to the mix, and the tube was incubated for 30 min in an incubator at 37 ℃ in 5% CO_2.

While the transfection mix was in the incubator, the cells were spun down and the media was aspirated (as described in section 3.1). A total of 16 100-mm cell culture plates were split into 8 groups, in which 4 groups would receive a transfection mix containing OE vector and 4 groups would receive a transfection mix containing empty vector (EV). Each group received a total of 334 µL of the designated transfection mix (167 µL x 2). Subsequently, the cells were replated in a total of 16 100-mm cell culture plates and incubated overnight in an incubator at 37 ℃ in 5% CO_2. The equivalent strategy was employed in the KD experiment.

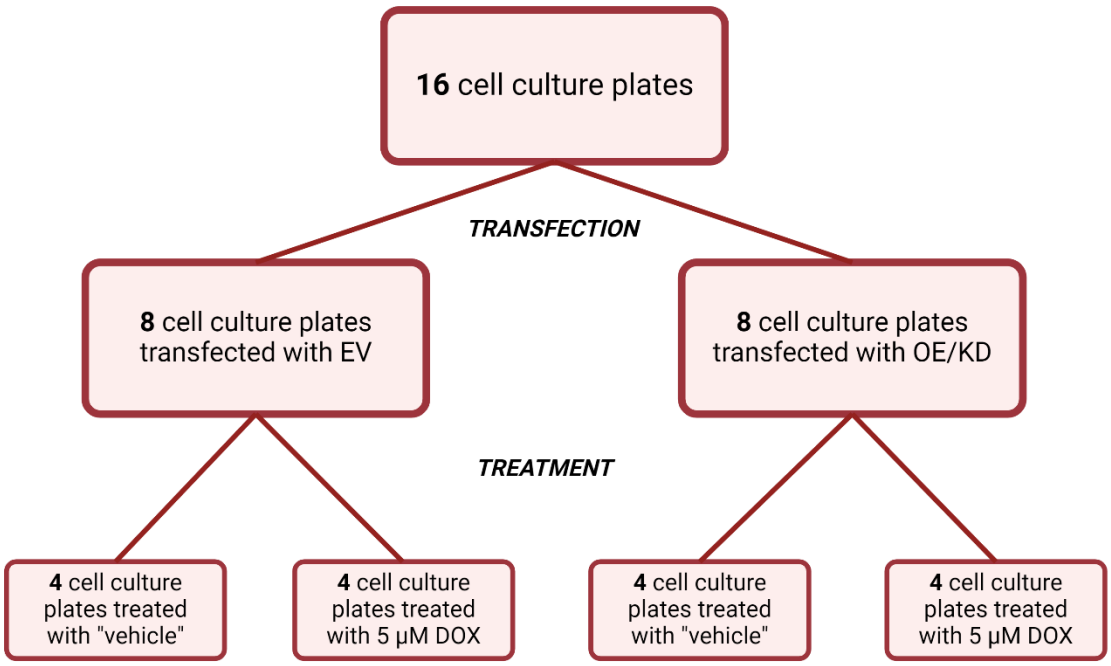

Figure 4. Schematic representation of the experimental paradigm. *A total of 16 100-mm cell culture plates containing AC-16 cardiomyocytes at ~ 80% confluency were split into two groups. One group was transfected with an empty vector (EV), and the other was transfected with either an overexpression (OE) or knockdown (KD) vector. Following overnight incubation at 37 ℃ in 5% CO_2, each group was further split into two subgroups, each consisting of four 100-mm cell culture plates (biological replicates). These subgroups were treated with either a "vehicle" medium or a 5 µM DOX medium for 24 hours at 37 ℃ in 5% CO_2. Created with BioRender.com.*

3.3 Doxorubicin treatment

A DOX concentration of 5 µM and a treatment duration of 24 hours were chosen for the experiment, and these parameters were based on findings from Berg et al. (63). Firstly, a 1 mM doxorubicin hydrochloride (DOX; Sigma Aldrich, Darmstadt, Germany) stock solution was prepared with sterile H_2O (B. Braun, Meisungen, Germany) as a diluent. Then, 250 µL 1 mM DOX stock solution was added to 49.75 mL culture medium, creating a 5 µM DOX medium solution. For the control groups, 250 µL sterile H_2O was added to 49.75 mL culture medium, creating a "vehicle" solution. A media change was performed on the cells, whereby waste media were aspirated and replaced with either 5 mL 5 µM DOX medium solution or 5 mL "vehicle" solution (Fig. 4). Then, the treated cell culture plates were incubated for 24 hours in an incubator at 37 ℃ in 5% CO_2. The equivalent strategy was employed for both OE and KD experiments.

3.4 Harvesting the cells and preparation of cell lysates

After 24-hours DOX treatment, cells were harvested, and cell lysates prepared. The condition medium was aspirated from each of the 16 100-mm cell culture plates, collected in 50-mL tubes and stored in a freezer at -18 ℃. Samples from the condition media were used in the LDH-release assay. Subsequently, 1 mL of non-denaturing lysis buffer was added to each plate, and the cells were collected in 1.5-mL tubes. Next, the lysed cells were centrifuged at 12,000 x g in 4 ℃ for 10 min in a centrifuge. Following centrifugation, cell lysate was separated from cell debris, and the cell lysate was collected in 1.5-mL tubes, while the cell debris was discarded. The prepared cell lysate samples were then stored in a freezer at -18 ℃.

3.5 Bradford assay

The Bradford assay is a rapid and sensitive method for determining total protein concentration in a sample utilizing the principle of protein-dye binding. This chemical assay employs a Coomassie G-250 dye, which upon protein binding undergoes a shift in absorption maximum, thereby facilitating the quantitative estimation of the protein concentration (64).

In the preparation of a standard curve, the initial step involved dissolving bovine serum albumin powder in MilliQ H_2O to generate a 10 mg/mL stock solution. This was followed by a 1:100 dilution in MilliQ H_2O, yielding a 100 µg/mL solution. Subsequently, serial 1:2 dilutions with MilliQ H_2O was performed to generate standard solutions labelled A-F. From each standard solution, 640 µL were transferred into new tubes labelled A1-F1, to which 160 µL of Bradford reagent (5x, Thermo Fisher Scientific, Waltham, MA, USA) were added. A control solution was prepared by mixing 640 µL of MilliQ H_2O with 160 µL of the Bradford reagent (5x) in a tube labelled G1. These solutions (A1-G1) now contained known protein concentrations.

The cell lysate samples were prepared by diluting 4 µL of each cell lysate in 12 µL of non-denaturing lysis buffer. Following dilution, 4 µL of this prepared cell lysate solution was further diluted with 636 µL of MilliQ H_2O. Subsequently, 160 µL of Bradford reagent (5x) was added to the mixture, resulting in a final volume of 800 µL for each sample. These samples, along with the previously prepared standard solutions were then plated in triplicate into a 96-well microplate, with each well receiving 200 µL of the solution. The absorbance was measured at 595 nm using a Varioskan LUX plate-reader (Thermo Fisher Scientific, Waltham, MA, USA). A standard curve, derived from the absorbance measurements of the standard solutions, was used to calculate the protein

concentrations in the cell lysate samples. Subsequently, this allowed for the normalization of the cell lysates, ensuring uniform protein input for later experiments.

3.6 MTT assay

The MTT assay is a cell metabolic activity assay that is frequently utilized to infer secondary cellular processes, such as cell viability. It relies on a chemical redox reaction, where the MTT reagent, 3-(4,5-dimethylthiazol-2-yl)-2,5-diphenyl-2H-tetrazolium bromide, is intracellularly reduced by oxidoreductase and dehydrogenase enzymes and electron donors into formazan. This water-insoluble compound is then solubilized by a solubilizing agent, typically after a few hours of incubation with the MTT reagent. A color change is observed after the reaction and subsequent solubilization, from yellow to violet, and the absorbance can be measured by a plate reader. The optical density value corresponds to the level of metabolic activity (65).

AC-16 cardiomyocytes were transfected as described in *section 3.2* and seeded in a 96-well microplate at a density of 20,000 cells per well. The first two rows (A and B) were seeded with EV-transfected AC-16 cardiomyocytes and the third and fourth row (C and D) were seeded with either OE-transfected or KD-transfected AC-16 cardiomyocytes. Four biological replicates (BRs 1-4) were prepared for each treatment group and each BR were plated in triplicate, i.e., BR 1 in wells 1-3, BR 2 in wells 4-6, and so on. In addition, the first three wells in rows G and H were filled with culture medium as controls. The 96-well microplate was incubated overnight at 37 ℃ in 5 % CO_2. Following this, rows B and D were treated with 5 µM DOX-medium for 24 hours, while rows A and C were treated with a "vehicle"-medium for 24 hours at 37 ℃ in 5 % CO_2. Row G was treated with "vehicle"-medium and Row H was treated with 5 µM DOX-medium as controls.

After 24 hours of incubation with the designated medium, 20 µL MTT reagent (Roche Diagnostics GmbH, Mannheim, Germany), was spiked to each well, and the 96-well microplate was incubated at 37 ℃ in 5 % CO_2 for 3 hours. Then, 100 µL Solubilization buffer (Roche Diagnostics GmbH, Mannheim, Germany), was spiked to each well and mixed thoroughly, before leaving the 96-well microplate at room temperature, shielded from light, overnight. Following this, the 96-well microplate was read by a Varioskan LUX plate-reader (Thermo Fisher Scientific, Waltham, MA, USA) and the absorbance measured at 570 nm.

3.7 Sandwich enzyme-linked immunosorbent assays (ELISAs)

A sandwich ELISA is a quantitative analytical method in which the analyte of interest, e.g., a protein or peptide, is captured by a capture antibody and then detected by a detection antibody that is linked to an enzyme. The presence of the analyte is confirmed by adding a suitable enzyme substrate that, when catalyzed, causes a color change; this change can be measured through absorbance to determine the quantity of the analyte (66). An illustration providing a basic overview of the principle of a sandwich ELISA is presented in Fig. 5. To validate the specificity of the sandwich ELISAs, a principle termed *specific peptide blocking* was performed. The peptide employed acts as a competitive inhibitor of the primary (detection) antibody when added in excess relative to it, thereby preventing the primary antibody from binding to its specific binding site on the analyte of interest. As such, the specific signal obtained from the detection of the analyte of interest is eliminated. Moreover, the signal detected in the wells where the blocking peptides were added is nonspecific and can be considered background noise. This background noise was eliminated from the obtained readings of the optical density value in the wells not subject

to *specific peptide blocking*. Hence, this value represents the actual signal in the detection of the analyte of interest.

The sandwich ELISAs performed in this study was done according to the procedure employed by Marwarha et al. (53). A list of the antibodies and antibody-blocking peptides utilized in this study is provided in Table 1.

Table 1. List of antibodies and antibody-blocking peptides utilized in this study.

Antibody	Use	Amount	Host	Manufacturer	Catalogue #
Akt	ELISA capture	10 ng/well	Mouse	Cell Signalling Technology	2920
Akt	ELISA detection	10 ng/well	Rabbit	Cell Signalling Technology	4691
p-Ser473 Akt	ELISA capture	10 ng/well	Mouse	Cell Signalling Technology	4051
p-Ser473 Akt	ELISA detection	10 ng/well	Rabbit	Cell Signalling Technology	9271
β-Actin	ELISA capture	20 ng/well	Mouse	Santa Cruz Biotechnology	sc-47778
β-Actin	ELISA detection	20 ng/well	Rabbit	Cell Signalling Technology	4970
β-Actin antibody blocking peptide	ELISA detection	N/A	N/A	Cell Signalling Technology	1025
Digoxigenin	ELISA capture	15 ng/well	Rabbit	R&D Systems	MAB10386
Goat Anti-Rabbit IgG-AP Conjugate	1:20000	N/A*	Goat	Sigma Aldrich/ Merck Life Science	A3687
GSK-3β	ELISA capture	10 ng/well	Mouse	Cell Signalling Technology	9832
GSK-3β	ELISA detection	10 ng/well	Rabbit	Cell Signalling Technology	9315
p-Ser9 GSK-3β	ELISA capture	10 ng/well	Mouse	Cell Signalling Technology	14630
p-Ser9 GSK-3β	ELISA detection	10 ng/well	Rabbit	Cell Signalling Technology	9322
LDH	ELISA capture	30 ng/well	Mouse	Santa Cruz Biotechnology	sc-133123
LDH-A	ELISA detection	30 ng/well	Rabbit	Novus Biologicals	NBP1-48336
LDH-A antibody blocking peptide	ELISA detection	N/A	N/A	Novus Biologicals	NBP1-48336PEP
LDH-B	ELISA detection	30 ng/well	Rabbit	Novus Biologicals	NBP2-38131
LDH-B antibody blocking peptide	ELISA detection	N/A	N/A	Novus Biologicals	NBP2-38131PEP

N/A: Not available/not applicable. *: Amount of secondary antibody cannot be determined as the commercial vendor does not provide the antibody concentration.

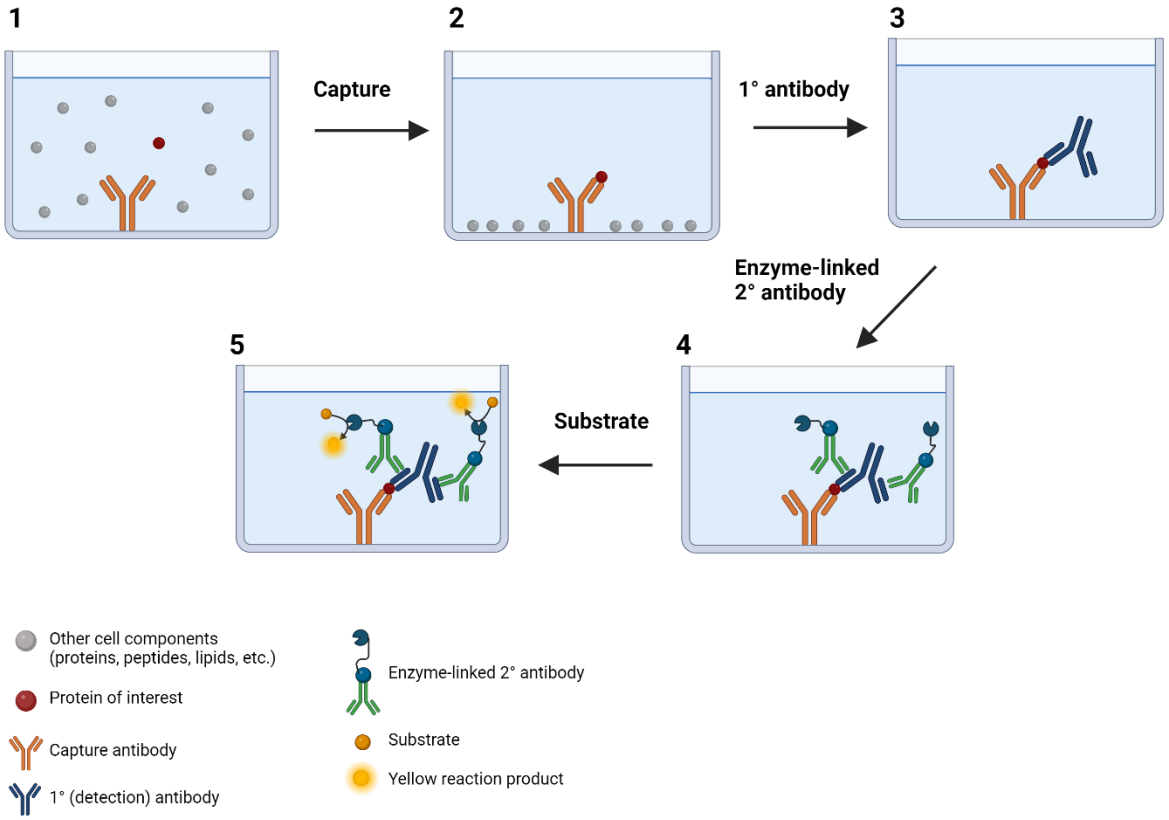

Figure 5. Basic overview of Sandwich ELISA. *(**1**) A sample is added into a well of a 96-well microplate precoated with capture antibody (one well is shown), and (**2**) the protein of interest is captured by the antibody upon incubation. Following washing with a washing buffer, (**3**) a detection (primary) antibody is added, and the plate is incubated. After washing with a washing buffer, (**4**) an enzyme-linked secondary antibody is added. The enzyme-linked secondary antibody binds to the primary antibody at multiple sites, leading to amplification of the signal. The plate is so incubated, before washing with a washing buffer. Then, (**5**) a substrate for the enzyme is added, before another incubation period. The substrate is converted from a colorless substance by the enzyme into a chromogenic reaction product, and the absorbance can be measured using a plate-reader. Created with BioRender.com.*

3.7.1 Lactate dehydrogenase (LDH)-release assay

The LDH-release assay measures the amount of the enzyme lactate dehydrogenase (LDH) released from damaged cells, providing a quantitative indication of general cell death (67). Firstly, 50 µL of the respective conditioned media and 150 µL PBS were added to each well of a precoated 96-well microplate. Then, the filled 96-well microplate was incubated overnight at 4 ℃. Subsequently, the conditioned media was discarded, and the 96-well microplate wells were washed 3 times (5 min each) with TBS-T (Tris-buffered saline with 0.1% v/v Tween-20). Following washing, the wells in rows A-D of the 96-well microplate were incubated with the LDH-A and LDH-B detection antibodies (Table 1), while the wells in rows E-H were incubated with the LDH-A and LDH-B detection antibodies + their respective antibody blocking peptides, overnight at 4 ℃. The 96-well microplate wells were then washed with TBS-T and incubated with the AP (alkaline phosphatase)-linked secondary antibody (Table 1) in room temperature, shielded from light, for 2.5 hours. Then, the 96-well microplate wells were washed with TBS-T and incubated with the AP-substrate PNPP (p-nitrophenyl phosphate, disodium salt) (Thermo Fisher Scientific, Oslo, Norway, Catalogue # 37621) in room temperature, shielded from

light, overnight. Subsequently, the absorbance at 405 nm was measured as previously described.

3.7.2 β-Actin ELISA immunoassay

The levels of β-actin in the cell lysates were quantified as an indicator of protein content in order to normalize the measured levels of the relevant analytes. Firstly, a volume corresponding to 10 µg of protein was taken out of each cell lysate sample and added to each well of a precoated 96-well microplate. Then, the filled 96-well microplate was incubated overnight at 4 ℃. Subsequently, the 96-well microplate wells were washed 3 times (5 min each) with TBS-T (Tris-buffered saline with 0.1% v/v Tween-20). After washing, the wells in rows A-D of the 96-well microplate were incubated with the β-actin detection antibodies (Table 1), while the wells in rows E-H were incubated the β-actin detection antibodies + antibody blocking peptide, overnight at 4 ℃. The 96-well microplate wells were then washed with TBS-T and incubated with the AP (alkaline phosphatase)-linked secondary antibody (Table 1) in room temperature, shielded from light, for 2.5 hours. Then, the 96-well microplate wells were washed with TBS-T and incubated with the AP-substrate PNPP (p-nitrophenyl phosphate, disodium salt) (Thermo Fisher Scientific, Oslo, Norway, Catalogue # 37621) in room temperature, shielded from light, overnight. Subsequently, the absorbance at 405 nm was measured as previously described.

3.7.3 GSK-3β, p-Ser9 GSK-3β, Akt, and p-Ser473 Akt ELISA immunoassays

Firstly, a volume corresponding to 10 µg of protein (GSK-3β and Akt) or 40 µg (p-Ser9 GSK-3β and p-Ser473 Akt) was taken out of each cell lysate sample and added to each well of a precoated 96-well microplate. Then, the filled 96-well microplate was incubated overnight at 4 ℃. Subsequently, the 96-well microplate wells were washed 3 times (5 min each) with TBS-T (Tris-buffered saline with 0.1% v/v Tween-20) and incubated with the respective detection antibodies (Table 1) overnight at 4 ℃. The 96-well microplate wells were then washed with TBS-T and incubated with the AP (alkaline phosphatase)-linked secondary antibody (Table 1) in room temperature, shielded from light, for 2.5 hours. Then, the 96-well microplate wells were washed with TBS-T and incubated with the AP-substrate PNPP (p-nitrophenyl phosphate, disodium salt) (Thermo Fisher Scientific, Oslo, Norway, Catalogue # 37621) in room temperature, shielded from light, overnight. Subsequently, the absorbance at 405 nm was measured as previously described.

3.8 Enzyme-linked miR-210 hybridization immunoassay

miR-210 levels in the experimental lysates was determined by a microRNA immunoassay method (68). The experimental lysates were added to a precoated 96-well microplate at an input of 20 µg of protein per well. Subsequently, the 96-well microplate was incubated with the experimental lysate at 4 ℃ overnight. Then, the 96-well microplate wells were washed 3 times (5 min each) with TBS-T (Tris-buffered saline with 0.1% v/v Tween-20) before adding a digoxigenin-labelled miR-210 LNA detection probe (Qiagen Norge, Oslo, Norway, Catalogue # 339412YCO0212945) solution to each well. This was followed by an overnight incubation at 4 ℃. Next, the 96-well microplate wells were washed 3 times (5 min each) with TBS-T before adding digoxigenin primary antibody solution and digoxigenin primary antibody + blocking peptide (Table 1) to rows A-D and E-H, respectively. The 96-well microplate was then subject to overnight incubation at 4 ℃. Following this, the 96-well microplate wells were washed 3 times (5 min each) with TBS-T

before adding secondary AP-conjugated antibody solution to each well. This was followed by incubation of the 96-well microplate on a shaker at room temperature, shielded from light, for 2.5 hours. Subsequently, after washing the 96-well microplate wells 3 times (5 min each) with TBS-T, the AP-substrate PNPP (p-nitrophenyl phosphate, disodium salt) (Thermo Fisher Scientific, Oslo, Norway, Catalogue # 37621) was added to each well. Then, the 96-well microplate was incubated on a shaker at room temperature, shielded from light, overnight. Lastly, the absorbance was measured at 405 nm as previously described.

3.9 Caspase-3 activity assay

The specific caspase-3 substrate Ac-DEVD-p-NA (n-Acetyl-Ac-Asp-Glu-Val-Asp-p-nitroanilide) is cleaved by caspase 3 and caspase 7 into a chromogenic reaction product, enabling colorimetric estimation of their activities (69). As caspase-3 is an effector caspase of the apoptotic cell death pathway, its activity is a strong indicator of apoptotic cell death.

Firstly, a volume corresponding to 100 µg of protein was taken out of each cell lysate sample and added to each well of a precoated 96-well microplate. In addition, the specific caspase-3 substrate Ac-DEVD-p-NA (Sigma Aldrich, Oslo, Norway, Catalogue # 235400-5MG) was added to each well in rows A-D and the substrate + inhibitor was added to each well in rows E-H. Then, the filled 96-well microplate was incubated in room temperature on a shaker, shielded from light, for 24 hours. Subsequently, the absorbance at 405 nm was measured as previously described.

3.10 Bioinformatics

A search for predicted hsa miR-210-3p target genes was performed in the TargetScanHuman 8.0 database (70). The identified predicted target genes were prompted along with Akt into the STRING 12.0 database (71) in order to identify the relationship between the predicted target genes and Akt.

3.11 Statistical analysis

All values are presented as means ± standard deviation (S.D.). Data were analyzed using GraphPad Prism (version 10.1.2) statistical software. Multiple comparisons between the different treatment groups were performed using one-way ANOVA with Tukey’s Post Hoc test. For all tests, a p-value of less than 0.05 was defined as statistically significant.

4 Results

4.1 miR-210 increases cell viability in DOX-treated AC-16 cardiomyocytes

To determine if upregulation or downregulation of miR-210 would affect the cell viability of AC-16 cardiomyocytes exposed to DOX treatment, an MTT assay was performed. The results showed that overexpression of miR-210 increased the cell viability of AC-16 cardiomyocytes treated with 5 μM DOX solution for 24 hours ($p < 0.05$; Fig. 6A). However, no statistically significant difference was observed in cell viability under unstimulated conditions ("vehicle" treatment) upon miR-210 overexpression (Fig. 6A). Knockdown of miR-210 did not affect cell viability in the DOX-treated group, nor under unstimulated conditions (Fig. 6B). These results indicate that miR-210 promotes the survival of DOX-treated AC-16 cardiomyocytes.

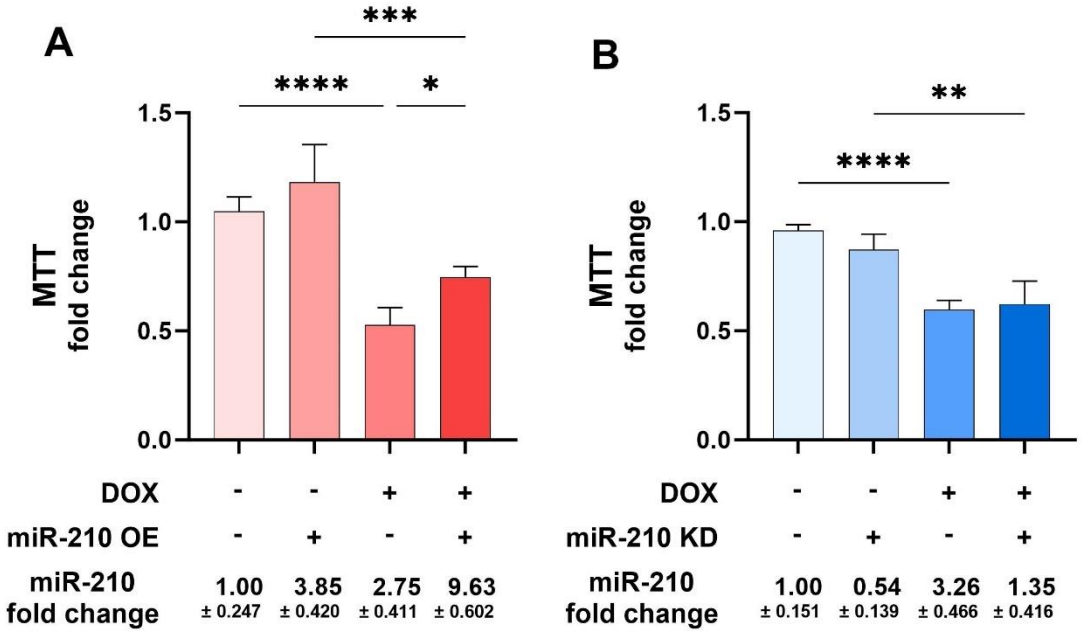

Figure 6. miR-210 increases cell viability in DOX-treated AC-16 cardiomyocytes. *3-(4,5-dimethylthiazol-2-yl)-2,5-diphenyl-2H-tetrazolium bromide (MTT) assays determining cell viability in AC-16 cardiomyocytes treated with 5 μM DOX medium after overexpressing miR-210 (OE) or downregulating miR-210 (KD). (**A**) Transfection with a miR-210 OE vector increased the cell viability in the DOX-treated group. (**B**) Transfection with a miR-210 KD vector did not affect the cell viability in the DOX-treated group. Absorbance was measured at 570 nm. All data are expressed as mean ± S.D. from three technical replicates for each of the four biological replicates belonging to each experimental group (n = 4). * $p < 0.05$; ** $p < 0.01$; *** $p < 0.001$; **** $p < 0.0001$. DOX: doxorubicin; OE: miR-210 overexpression; KD: miR-210 knockdown; S.D.: standard deviation.*

4.2 miR-210 reduces cell death in DOX-treated AC-16 cardiomyocytes

To determine if upregulation or downregulation of miR-210 would affect cell death in AC-16 cardiomyocytes exposed to DOX treatment, an LDH-release assay was performed. Overexpression of miR-210 reduced the LDH release ($p < 0.001$; Fig. 7A), while downregulation of miR-210 augmented the LDH release ($p < 0.0001$; Fig. 7B) in the condition media after being treated with 5 µM DOX medium for 24 hours. These results indicate that miR-210 reduces cell death in DOX-treated AC-16 cardiomyocytes.

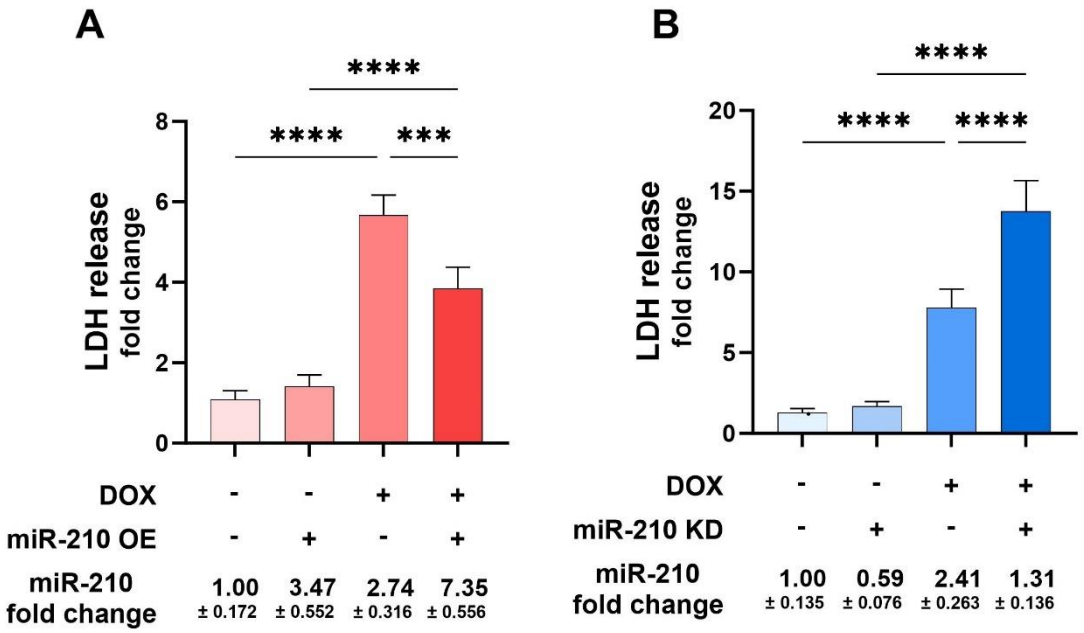

Figure 7. Overexpression and downregulation of miR-210 affect cell death in DOX-treated AC-16 cardiomyocytes. *(**A**) miR-210 overexpression significantly reduced general cell death, while (**B**) miR-210 downregulation significantly increased general cell death, as measured by a lactate dehydrogenase (LDH) release assay. Absorbance was measured at 405 nm. All data are expressed as mean ± S.D. from three technical replicates for each of the four biological replicates belonging to each experimental group (n = 4). *** $p < 0.001$; **** $p < 0.0001$. DOX: doxorubicin; LDH: lactate dehydrogenase; OE: miR-210 overexpression; KD: miR-210 knockdown; S.D.: standard deviation*.

4.3 miR-210 inhibits apoptosis in DOX-treated AC-16 cardiomyocytes

After having observed that miR-210 reduces general cell death, caspase-3 activity was measured to determine if this effect could, at least in part, be explained by an effect on apoptotic cell death. Overexpression of miR-210 significantly reduced caspase-3 activity in AC-16 cardiomyocytes exposed to 5 µM DOX medium ($p < 0.0001$), while no difference in caspase 3 activity was observed in the unstimulated ("vehicle"-treated) group ($p > 0.05$; Fig. 8A). An increase in caspase 3 activity was observed after downregulation of miR-210 in the DOX-treated group ($p < 0.0001$), while no difference in caspase 3 activity was observed in the unstimulated group ($p > 0.05$; Fig. 8B). These

results indicate that miR-210 inhibits cell death in AC-16 cardiomyocytes through modulating apoptosis. An additional observation is that DOX treatment itself induces expression of miR-210 and increases its intracellular levels by approximately 2.5-fold (Fig. 8A and B).

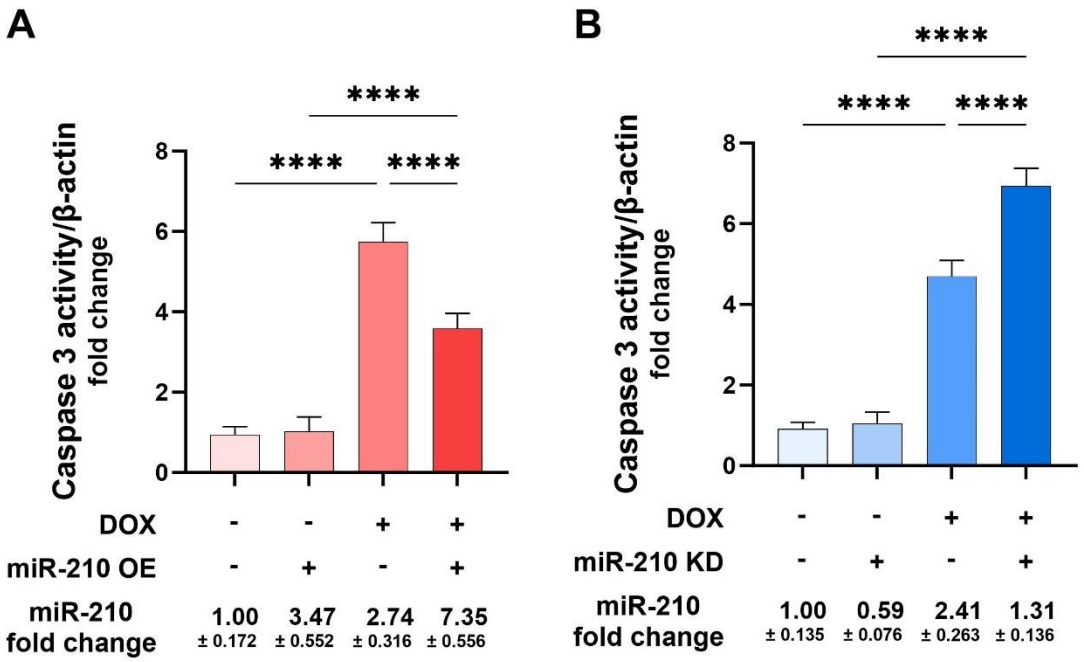

Figure 8. miR-210 reduces DOX-induced apoptotic cell death in AC-16 cardiomyocytes*. (**A**) Overexpressing miR-210 significantly attenuated caspase-3 activity, while (**B**) knocking down miR-210 significantly increased caspase-3 activity. Absorbance was measured at 405 nm. All data are expressed as mean ± S.D. from three technical replicates for each of the four biological replicates belonging to each experimental group (n = 4). **** p < 0.0001. DOX: doxorubicin; OE: miR-210 overexpression; KD: miR-210 knockdown; S.D.: standard deviation.*

4.4 miR-210 inhibits DOX-induced apoptotic cell death by affecting phosphorylation status of GSK-3β

As previous studies have shown that miR-210 modulates hypoxia-induced apoptosis by affecting the phosphorylation status of GSK-3β at serine 9 (Ser9), it was explored if a similar mechanism might underlie the miR-210-mediated decrease in DOX-induced apoptosis. In the first phase of our investigation, we quantified the levels of GSK-3β protein in lysates derived from DOX-treated AC-16 cardiomyocytes, either transfected with an overexpression (OE) vector or a knockdown (KD) vector. No significant difference in protein expression levels of GSK-3β were observed across the two experiments (Fig. 9A and B). Subsequently, we assessed the phosphorylation status of GSK-3β (p-Ser9 GSK-3β) relative to GSK-3β protein levels. Transfection with a miR-210 OE vector caused a significant increase in p-Ser9 GSK-3β compared to the EV control group after DOX treatment ($p < 0.0001$; Fig. 9C). In contrast, no significant difference in relative p-Ser9 GSK-3β levels was observed when miR-210 was knocked down as compared to the EV control group after DOX treatment ($p > 0.05$; Fig. 9D). These results indicate that miR-210 increases phosphorylation of GSK-3β at Ser9 when exposed to DOX.

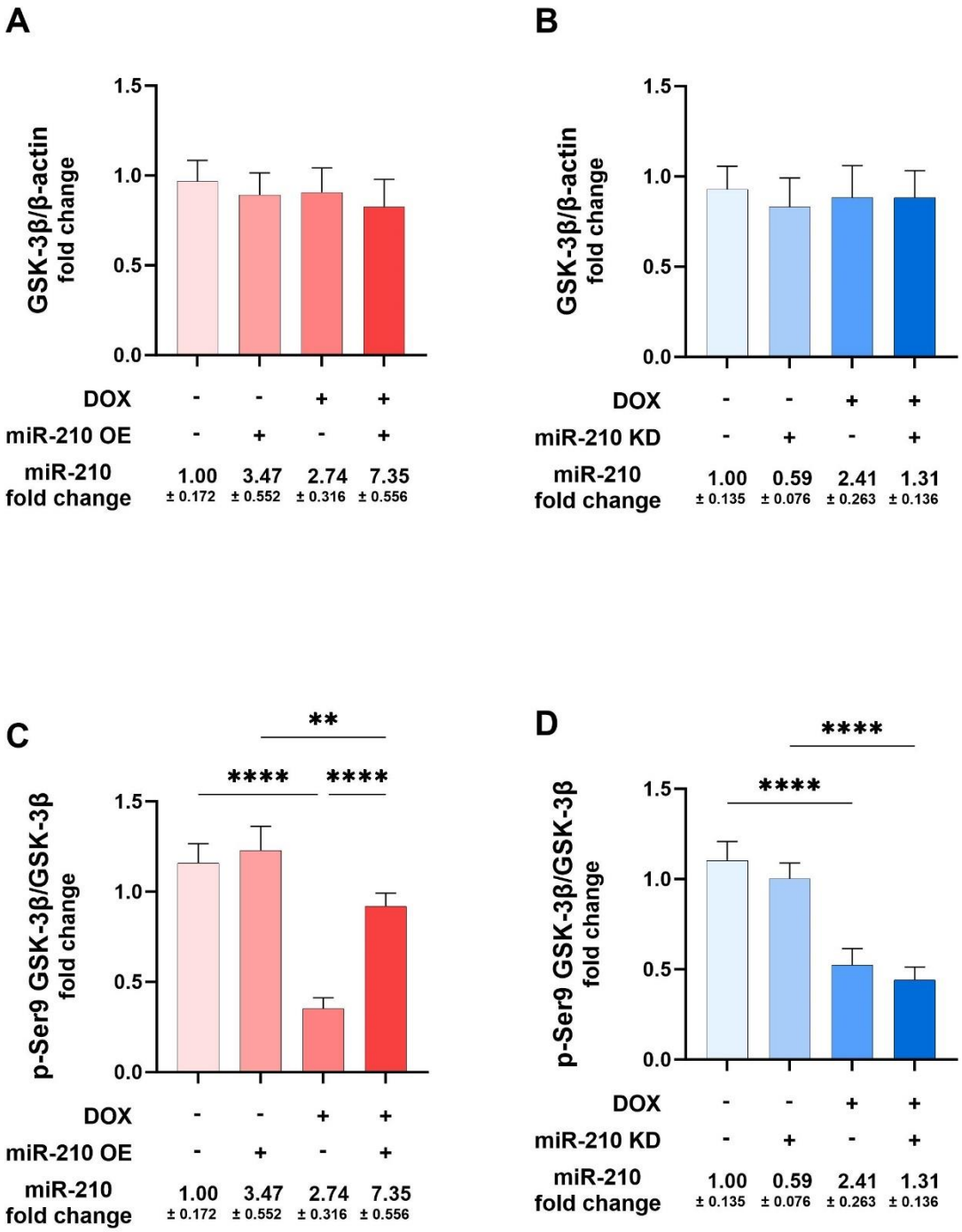

Figure 9. miR-210 overexpression increases phosphorylation at serine 9 residue (Ser9) of glycogen synthase kinase-3β (GSK-3β) in DOX-treated AC-16 cardiomyocytes. *No change in protein expression levels of GSK-3β were observed in AC-16 cardiomyocytes transfected with an overexpression (OE) vector (**A**) nor a knockdown (KD) vector (**B**) of miR-210 across all treatment arms. (**C**) Phosphorylation at Ser9 of GSK-3β is increased with miR-210 OE vector as compared to EV after 24-hours DOX treatment. (**D**) No significant difference in phosphorylation at Ser9 of GSK-3β is observed with miR-210 KD vector as compared to EV after 24-hours DOX treatment. Absorbance was measured at 405 nm. All data are expressed as mean ± S.D. from three technical replicates for each of the four biological replicates belonging to each experimental group (n = 4). ** p < 0.01; **** p < 0.0001. DOX: doxorubicin; OE: miR-210 overexpression; KD: miR-210 knockdown; S.D.: standard deviation.*

4.5 miR-210 affects phosphorylation status of Akt in DOX-treated AC-16 cardiomyocytes

Akt has a known inhibitory effect on GSK-3β activity by phosphorylation at Ser9, and as such, it was explored if altered Akt expression or activity might underlie the observed difference in p-Ser9 GSK-3β levels in miR-210 OE transfected AC-16 cardiomyocytes exposed to DOX. In the first phase of our investigation, we quantified the levels of Akt protein in lysates derived from DOX-treated AC-16 cardiomyocytes, either transfected with an overexpression (OE) vector or a knockdown (KD) vector. No significant difference in protein expression levels of Akt were observed across the two experiments (Fig. 10A and B). Then, the phosphorylation status of Akt (p-Ser473 Akt) were measured relative to Akt protein levels. Transfection with a miR-210 OE vector caused a significant increase in p-Ser473 Akt as compared to the EV control group after DOX treatment ($p < 0.01$; Fig. 10C). Meanwhile, transfection with a miR-210 KD vector caused a significant decrease in p-Ser473 as compared to the EV control group after DOX treatment ($p < 0.05$; Fig. 10D).

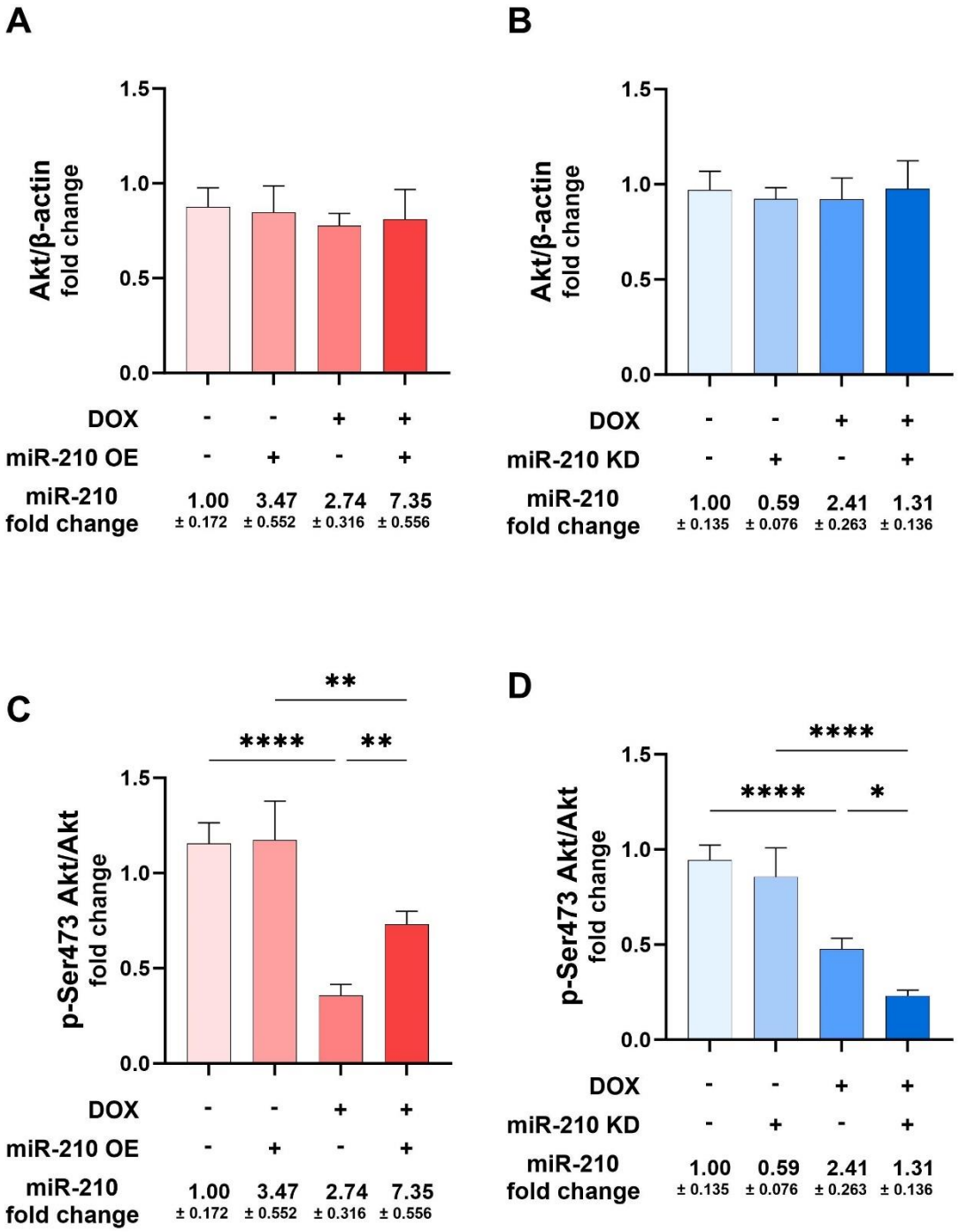

Figure 10. miR-210 affects phosphorylation of Akt at serine 473 (Ser473) in DOX-treated AC-16 cardiomyocytes. *No change in protein expression levels of Akt were observed in AC-16 cardiomyocytes transfected with an overexpression (OE) vector (**A**) nor a knockdown (KD) vector (**B**) of miR-210 across all treatment arms. (**C**) Phosphorylation at Ser473 of Akt is increased with miR-210 OE vector as compared to EV after 24-hours DOX treatment. (**D**) A significantly lower degree of phosphorylation at Ser473 of Akt is observed with miR-210 KD vector as compared to EV after 24-hours DOX treatment. Absorbance was measured at 405 nm. All data are expressed as mean ± S.D. from three technical replicates for each of the four biological replicates belonging to each experimental group (n = 4). * p < 0.05; ** p < 0.01; **** p < 0.0001. DOX: doxorubicin; OE: miR-210 overexpression; KD: miR-210 knockdown; S.D.: standard deviation.*

4.6 Predicted miR-210 target genes and their relationship to Akt

The results presented so far indicate that miR-210 inhibits DOX-induced apoptotic cell death by affecting Akt, not by modulating its protein expression levels but by increasing its phosphorylation status (p-Ser473 Akt). Hence, Akt can be characterized as an indirect target of miR-210. As such, a bioinformatical analysis was performed to identify direct miR-210 target genes that would provide a link to Akt and its activation status (Fig. 11). Several predicted target genes were found to have an experimentally determined connection to Akt. These included *EFNA3*, *RAP2B*, *BDNF*, *ATG7*, *HIF3A*, *KMT2D*, and *E2F3*. Others were found to have a more indirect link to Akt (based on textmining; Fig. 11). While the rest were not identified as having a connection with Akt.

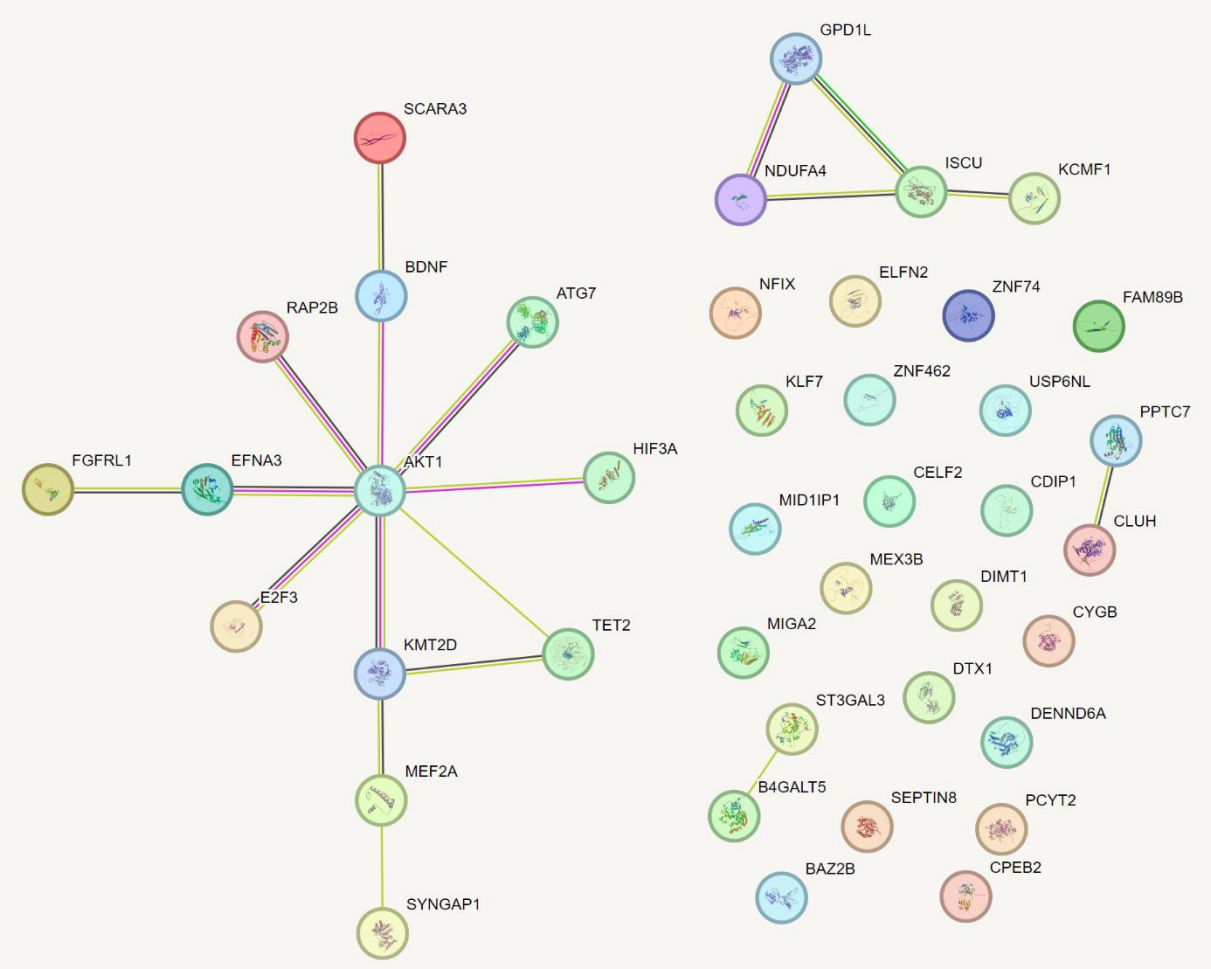

Figure 11. Predicted miR-210 target genes and their relationship to Akt*. The predicted hsa-miR-210-3p target genes according to TargetScanHuman 7.2 were plotted into the STRING 12.0 database alongside Akt to identify their relationship with Akt. EFNA3, RAP2B, BDNF, ATG7, HIF3A, KMT2D, and E2F3 (pink lines) were all identified as having an experimentally determined relationship to Akt. SCARA3, TET2, MEF2A, SYNGAP1, and FGFRL1, on the other hand, were identified as having a more indirect relationship to Akt (green lines). Green lines indicate a protein-protein association based on textmining. The rest were not identified as having a relationship to Akt (target genes on the right hand-side).*

5 Discussion

With the rise in cancer survivor rates, the long-term cardiac side effects associated with cancer treatments are becoming increasingly apparent. DOX, a widely used chemotherapeutic drug, is notably associated with cardiotoxicity as a side effect. DOX-induced cardiotoxicity is characterized by a reduction in left ventricular ejection fraction exceeding 10%, resulting in a final left ventricular ejection fraction value below 53% (72). Currently, there are few treatment options for DOX-induced cardiotoxicity, with dexrazoxane being the only FDA-approved drug for this indication (73). Meanwhile, miRNAs have gained attention as important regulators of numerous cellular processes in recent years. One of these miRNAs, miR-210, has been shown to play a protective role in models of ischemic heart disease (74). In this study, upregulation and downregulation of miR-210 were performed to determine its effect on cell death, cell viability, apoptosis, and to explore the involvement of the Akt-GSK-3β pathway in human AC-16 cardiomyocytes exposed to 5 μM DOX for 24 hours.

5.1 Effects of miR-210 on DOX-induced AC-16 cardiomyocyte death

It is well-known that DOX has a deleterious impact on cell viability (31, 63, 75). This is consistent with the results from this study. Interestingly, the upregulation of miR-210 was found to significantly reduce the decrease in cell viability caused by DOX. Previous studies have demonstrated that miR-210 promotes the survival and proliferation of human cardiomyocytes upon ischemia/reperfusion injury (76). Another study demonstrated that modulating miR-210 directly affects the viability of neural progenitor cells in hypoxic conditions. Upregulating miR-210 enhances cell viability, while downregulating it leads to decreased viability under identical hypoxic stress (52). Our findings suggest that miR-210 plays a protective role upon DOX-induced stress in human AC-16 cardiomyocytes, in line with previous reports examining the role of miR-210 under other stress-induced conditions such as oxygen-glucose deprivation/reperfusion and anoxia (74, 77). Moreover, no difference in cell viability was observed between the miR-210 OE- or KD-transfected cells and the EV-transfected cells in nonstimulated (“vehicle”) conditions, suggesting that miR-210 does not affect cell viability in any direction when not exposed to stressful conditions. This is also in line with a study showing that upregulation of miR-210 did not affect cell viability under normoxic conditions (52). Moreover, since cardiomyocyte death is considered to be a primary event in DOX-induced cardiac damage (11), an LDH-release assay was performed to assess the effects of miR-210 on general cell death. Previous studies have shown a concentration- and time-dependent effect of DOX-induced cell death in AC-16 cardiomyocytes (78). In this study, 5μM DOX-treatment for 24 hours induced a 6-8-fold increase in LDH release, implying a substantial rise in general cell death, in line with the results from the MTT-assay.

The ROS, DNA double-strand breaks, and other molecular events triggered by DOX lead to induction of apoptosis. In this study, caspase-3 activity was measured as a surrogate of apoptotic cell death. The results showed that treatment of AC-16 cardiomyocytes with 5μM DOX for 24 hours caused a significant increase in caspase-3 activity. In neonatal rat cardiomyocytes, miR-210 has been shown to decrease mitochondrial ROS production under antimycin A-treated and hypoxic conditions (79). Additionally, in an *in vitro* oxygen glucose deprivation/reperfusion injury model, caspase-3 activity was reduced in cardiomyocytes transfected with miR-210 mimic (77). Since miR-210 has been implicated in reduced mitochondrial ROS production and inhibition of apoptosis under hypoxic stress

conditions, we wanted to test if miR-210 would also affect apoptosis under DOX-induced stress conditions. Indeed, upregulation of miR-210 significantly decreased caspase-3 activity in DOX-treated cells, while downregulation of miR-210 significantly increased caspase-3 activity, implicating a role of miR-210 in modulating apoptotic cell death in DOX-treated cardiomyocytes.

GSK-3β is known to affect both the intrinsic and extrinsic apoptotic pathways, but in opposite directions. Increased inhibitory phosphorylation at p-Ser9 of GSK-3β mediates a decrease in the activation of the intrinsic apoptotic pathway, while augmenting the initiation of the extrinsic apoptotic pathway (58). The magnitude of these effects depends on the prevailing signaling pathways activated in the cell. In this study, a caspase-3 activity assay was performed to study the effects of miR-210 on apoptotic cell death in AC-16 cardiomyocytes exposed to DOX. As caspase-3 activity is strongly correlated with apoptotic cell death, the increase in caspase-3 activity upon treatment with 5μM DOX for 24 hours, suggests that apoptotic cell death plays a major role in DOX-induced cell death. However, since caspase-3 is a pivotal effector caspase in both the intrinsic and the extrinsic apoptotic pathways, this assay is nonspecific with respect to which pathway prevails under DOX-induced stress conditions. Nonetheless, upregulation of miR-210 caused a reduction in caspase-3 activity and an increase in phosphorylation at p-Ser9 of GSK-3β, a finding indicating that miR-210 decreases intrinsic apoptotic cell death in DOX-treated AC-16 cardiomyocytes. This finding is in line with a recent study by Marwarha et al. identifying GSK-3β as a distal molecular target of miR-210 (54). Moreover, downregulation of miR-210 caused an increase in caspase-3 activity but did not cause a significant difference in phosphorylation at p-Ser9 of GSK-3β, a finding indicating augmented apoptotic cell death independent of p-Ser9 status of GSK-3β.

To further assess the observed increase in p-Ser9 status of GSK-3β upon upregulation of miR-210, a known regulator of GSK-3β, Akt, was studied. The protein expression levels of Akt were not affected by DOX treatment, and neither upregulation nor downregulation of miR-210 caused any difference in the protein expression levels of Akt. Thus, levels of p-Ser473 Akt were examined to determine if any changes in Akt activity had occurred. Indeed, the p-Ser473 Akt-status was altered by DOX treatment, decreasing significantly as compared to vehicle treatment. This finding is in line with a previous study showing that ratio of p-Ser473 Akt/Akt in rat heart tissue, rat cardiomyocytes, and H9c2 cells was suppressed by DOX stimulation (59). Moreover, this observation might explain the decrease in inhibitory phosphorylation at Ser9 on GSK-3β. Furthermore, upregulation of miR-210 led to a significant increase in p-Ser473 Akt-status upon DOX treatment, while downregulation of miR-210 led to a significant decrease in p-Ser473 Akt-status. As such, our data support a role of miR-210 in regulating Akt activity at a post-translational level in DOX-treated AC-16 cardiomyocytes. Even though several other kinases are known to phosphorylate GSK-3β on the inhibitory Ser9 residue, the PI3K-Akt signaling pathway often acts as a major regulator of GSK-3β activity (58). Thus, our findings indicate that miR-210 inhibits apoptotic cell death in DOX-treated AC-16 cardiomyocytes by increasing p-Ser473 Akt-status, causing an increase in inhibitory phosphorylation at Ser9 in GSK-3β.

5.2 Predicted miR-210 target genes and Akt

To explore the potential molecular mechanism of the observed miR-210-induced increase in p-Ser473 Akt levels, an *in silico* search of potential gene targets was performed. A total of seven target genes were wound to have an experimentally determined relationship with Akt and where therefore selected as candidate genes for providing a link between miR-210 and the observed effect on p-Ser473 Akt-status in this study. These were as follows: *KMT2D*, *EFNA3*, *E2F3*, *RAP2B*, *BDNF, ATG7*, and *HIF3A*.

The gene *KMT2D* encodes the protein lysine methyltransferase 2D (KMT2D), which is a histone methyltransferase. Shangguan et al. found that knockdown of KMT2D in a murine chondrogenic cell line increases the phosphorylation status of p-Ser473 Akt (80). Given that *KMT2D* is a predicted target gene of miR-210, an upregulation of miR-210 would theoretically result in the downregulation of KMT2D protein expression levels. This decrease could consequently influence the phosphorylation status of p-Ser473 Akt in a similar manner. The same argument can be made for the predicted miR-210 target gene *EFNA3*. This gene encodes the protein ephrin A3 (EFNA3), which is a member of the ephrin family of cell-surface bound ligands. Findings from Bei et al. demonstrate that miR-210-mediated attenuation of oxygen-glucose deprivation/reperfusion-induced apoptosis in both neonatal rat cardiomyocytes and AC-16 cardiomyocytes is, in part, explained by an effect on EFNA3 (76). Furthermore, Zhuang et al. found that miR-210 promoted angiogenesis in human umbilical vein endothelial cells by suppression of EFNA3 expression (81). In the same study, the researchers demonstrated that knockdown of EFNA3 caused an increase in relative p-PI3K and p-Akt levels. Thus, these studies provide a link connecting miR-210 to inhibition of apoptosis and increased Akt activity, respectively. Consequently, *EFNA3* seems like a plausible candidate target gene for mediating the observed effects of miR-210 upregulation on p-Ser473 Akt levels in this thesis.

In an experimental study by Xu (82), it was found that downregulation of ten-eleven translocation 2 (TET2) in a rat model of coronary heart disease diminished cardiomyocyte apoptosis. Furthermore, this study showed that TET2 to promotes miR-126 expression in myocardial tissues of rats with coronary heart disease. This increase in miR-126 expression levels led to suppression of its identified gene target, the transcription factor *E2F3*, resulting in reduced E2F3 expression levels and an associated increase in cardiomyocyte apoptosis. Additionally, Xu's study included an experiment in which E2F3 was overexpressed to observe its effects on the PI3K-Akt signaling pathway. The overexpression of E2F3 was associated with a reduction in the phosphorylation status of PI3K and Akt compared to the control. Xu proposed that activation of the PI3K-Akt pathway in this context exacerbates coronary heart disease. As *E2F3* is a predicted gene target of miR-210 and overexpression of E2F3 is associated with inactivation of the PI3K-Akt pathway, the observed increase in p-Ser473 Akt levels in this thesis might be a consequence of miR-210-mediated suppression of E2F3 expression. On the other hand, as downregulation of another predicted miR-210 target gene, *TET2*, was correlated with a decrease in the activation of the PI3K-Akt pathway and a reduction in cardiomyocyte apoptosis, the effects of miR-210-mediated suppression of TET2 in DOX-induced cardiotoxicity are difficult to predict.

Cui et al. overexpressed the miRNA miR-205 in murine TM3 cells after identifying *RAP2B* (RAP2B, member of RAS oncogene family) as a target gene (83). They then explored the protein expression levels of PI3K, Akt, and p-Akt in TM3 cells transfected with miR-205,

finding a correlation between reduced RAP2B levels and decreased protein expression of PI3K, Akt, and p-Akt. Since *RAP2B* also is a predicted target gene of miR-210, these results might indicate that RAP2B does not mediate the increase in p-Ser473 Akt levels observed in this thesis. Another predicted miR-210 target gene, *BDNF*, which encodes the protein brain derived neurotrophic factor (BDNF), might fall into the same category as *RAP2B* with respect to affecting Akt activity. In a study by Zhao et al., inhibition of the long noncoding RNA BDNF-AS, an RNA molecule antisense to BDNF, caused an increase in murine cardiomyocyte survival exposed to hypoxia/reoxygenation injury (84). This effect was associated with an increase in BDNF protein expression levels and increased Akt phosphorylation. Thus, theoretically, a reduction in BDNF protein expression levels due to direct miR-210 targeting might result in reduced Akt phosphorylation. Hence, based on this finding, *BDNF* as a miR-210 target gene seems unlikely to cause the effects on p-Ser473 Akt levels observed in this thesis.

The *ATG7* gene encodes the autophagy-related protein 7 (ATG7), an enzyme involved in cellular autophagy. Zhao et al. demonstrated that ATG7 modulates p-Ser473 Akt levels through the cellular Jun-Phosphatase and Tensin Homolog pathway in HepG2 cells (85). Silencing of ATG7 using small interfering RNA caused an increase in p-Ser473 Akt levels. As a predicted miR-210 target gene, this might explain the increase in p-Ser473 Akt levels reported in this thesis when miR-210 was upregulated in DOX-treated AC-16 cardiomyocytes.

The last identified predicted miR-210 target gene is *HIF3A,* which encodes the hypoxia inducible factor 3 subunit alpha (HIF3A). By employing an *in vitro* model of chronic intermittent hypoxia in rat pulmonary artery smooth muscle cells, Xu et al. showed that silencing HIF3A using a small interfering RNA was associated with a decrease in p-PI3K and p-Akt protein levels (86). In that study, *HIF3A* was identified as a target gene of miR-485-5p, and overexpression and knockdown of miR-485-5p resulted in a reduction and an increase in HIF3A levels, respectively. If a similar mechanism were to take place in AC-16 cardiomyocytes, then an argument could be made stating that miR-210 targeting of HIF3A would result in reduced p-Akt protein levels, thus not an increase, as observed in this thesis.

Based on our findings from the *in silico* search for predicted miR-210 target genes and on the published literature, though an exhaustive literature review was not performed, *KMT2D*, *EFNA3*, *E2F3*, and *ATG7* stand out as plausible direct miR-210 target genes responsible for mediating the observed increase in p-Ser473 Akt status upon upregulation of miR-210 in DOX-treated AC-16 cardiomyocytes. A proposed mechanism for the miR-210-mediated reduction in caspase-3 activity observed in this thesis is provided in Fig. 12.

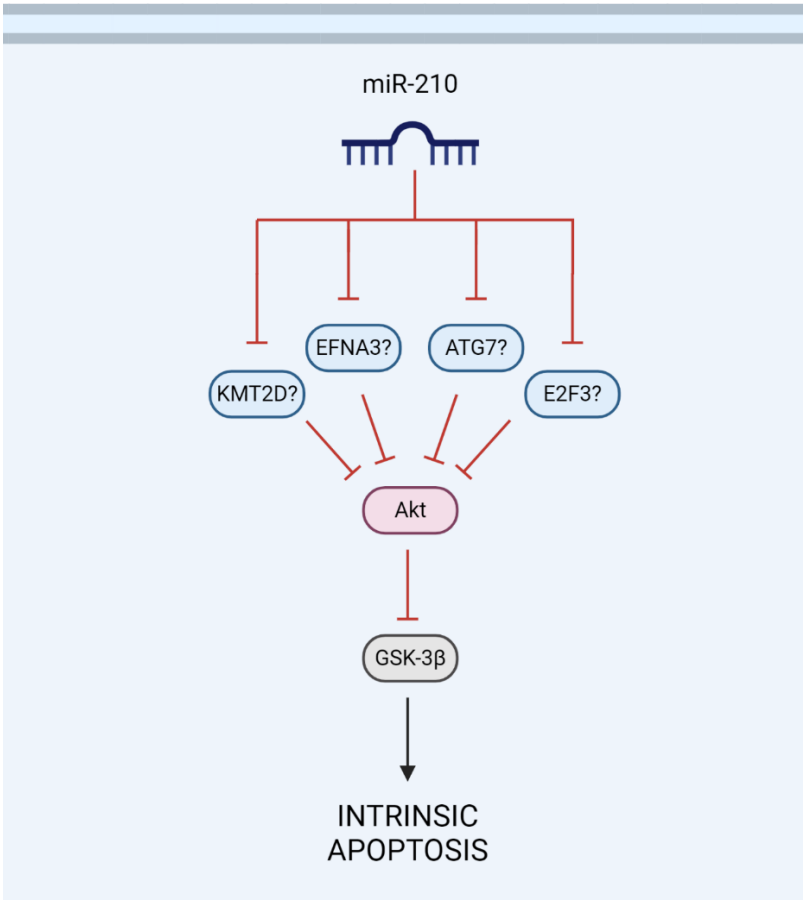

Figure 12. Proposed protective mechanism of upregulation of miR-210 in DOX-treated AC-16 cardiomyocytes. *miR-210 binds to the 3' untranslated region in the mRNA of one or more of its predicted target genes. This binding leads to the degradation of the mRNA and/or suppression of mRNA translation, resulting in reduced protein expression. Reduced protein expression of one or more of the predicted miR-210 target genes eventually causes an increase in phosphorylation of Akt at Ser473, activating this protein kinase. This, in turn, leads to an increase in the inhibitory phosphorylation of glycogen synthase kinase 3β (GSK-3β) at Ser9, which reduces the activation of the intrinsic apoptotic cascade, thereby rescuing cardiomyocytes exposed to DOX. Abbreviations: ATG7: autophagy related 7; DOX: doxorubicin; E2F3: E2F transcription factor 3; EFNA3: ephrin A3; KMT2D: lysine methyltransferase 2D; Ser: serine. Created with BioRender.com*

5.3 Future perspectives

DOX treatment itself induced the transcription of miR-210, with an observed increase of 2-3-fold. As miR-210 is known as a master *hypoxamiR* and acts as a central regulator in reprogramming cells under hypoxic conditions, our findings seem to suggest a protective role also under the influence of DOX-induced stress conditions. In hypoxic conditions, it is the HIF-1α transcriptional induction of miR-210 that accounts for most of the increase in miR-210 levels (50). How miR-210 is transcriptionally induced under DOX-induced stress remains unresolved and prompt further research.

As previously mentioned in this thesis, DOX-induced cell death is complicated and seems to involve a multitude of cell death mechanisms. One of these mechanisms, pyroptosis –

a caspase-mediated programmed form of necrosis (19) – has also been linked to DOX-induced cytotoxicity (18). Furthermore, pyroptosis has also been associated with the GSK-3β signaling pathway, and ticagrelor has been shown to inhibit pyroptosis in rat cardiomyocytes through the GSK-3β-caspase-1 pathway (59). This effect was shown to be cardioprotective. This raises the question of whether miR-210 might also influence cell death in DOX-treated cardiomyocytes by suppressing other cell death pathways, such as the pyroptotic cell death pathway. Although apoptosis has been the focal point in previous research as the final step leading to cardiomyocyte death in DOX-induced cardiotoxicity, attention has expanded, and evidence from studies implicating other cell death mechanisms is accumulating. Necroptosis and necrosis, for instance, together cause more cell death than apoptosis (87).

Cancer patients undergoing DOX treatment require strategies that do not compromise the drug's antitumor efficacy. Moreover, miR-210 exhibits dual roles in cancer biology: it acts as a tumor suppressor in some cancers, such as ovarian cancer, while demonstrating oncogenic activity in others, like breast cancer (88). miR-210 is overexpressed in numerous cancer types, aligning with its role in hypoxic cells within the tumor microenvironment (88). Thus, developing a strategy to target miR-210 specifically to the heart via a specialized drug delivery system might prevent adverse effects on cancer treatment outcomes in such a scenario.

5.4 Limitations

AC-16 cardiomyocytes were chosen as the cell line used in the experiments for this thesis. This choice was primarily due to their possession of a human genome, ease of genetic modification, and ability to produce large amounts of biological samples. However, as this cell line lacks some inherent properties found in primary cardiomyocytes, such as a functional electrophysiological machinery (61), the findings presented in this thesis may not perfectly reflect events in primary cardiomyocytes.

The DOX concentration and treatment duration chosen in this thesis was based on findings from Berg et al. (63). There is evidence implying that different cell death mechanisms prevail under different DOX concentrations. At higher concentrations, necrosis predominates, while at lower concentrations, apoptosis seems to be the dominant mechanism responsible for cell death (38). Additionally, the chosen concentration of 5 μM differs significantly form clinically relevant blood concentrations in human patients, which are typically in the range of 0.025-0.250 μM (72). These factors should be taken into consideration when interpreting the results presented in this thesis, as only one concentration and treatment duration were examined. Further studies are therefore warranted to fully elucidate the effects of miR-210 on cardiomyocyte survival when exposed to DOX.

Only one database was employed in the search for potential miR-210 target genes. However, some studies and websites list other target genes believed to affect apoptosis (52, 89). Some studies have implicated *BINP3* (52) *Casp8ap2* (74) as direct miR-210 target genes responsible for its role in inhibiting apoptosis. These targets were not listed in the database employed in this thesis. Additionally, the literature search performed to support the *in silico* miR-210 target gene prediction was not exhaustive. Therefore, there is a possibility that some significant links connecting the predicted miR-210 target genes and Akt, as well as the ways in which their gene products affect Akt activity, were missed in this thesis. Moreover, only a few of the studies referred to in section 5.2 actually used

a cardiomyocyte cell line, indicating that the predictions presented here might be confounded by the type of cell line used.

6 Conclusion

This thesis has demonstrated that miR-210 plays a protective role in AC-16 cardiomyocytes exposed to 5μM DOX treatment for 24 hours with respect to general cell death and cell viability. Additionally, it was shown that overexpression of miR-210 under these experimental conditions reduced caspase-3 activity, strongly indicative of reduced apoptotic cell death. This finding was associated with an increase in p-Ser473 Akt and p-Ser9 GSK-3β levels, implicating a role of these kinases as indirect targets of miR-210 in mediating this effect. Thus, this thesis suggests a novel role of miR-210 in mitigating DOX-induced cardiomyocyte death, highlighting its potential as a therapeutic target.

7 References

1. McGowan JV, Chung R, Maulik A, Piotrowska I, Walker JM, Yellon DM. Anthracycline Chemotherapy and Cardiotoxicity. Cardiovasc Drugs Ther. 2017;31(1):63-75.
2. Sritharan S, Sivalingam N. A comprehensive review on time-tested anticancer drug doxorubicin. Life Sci. 2021;278:119527.
3. Mattioli R, Ilari A, Colotti B, Mosca L, Fazi F, Colotti G. Doxorubicin and other anthracyclines in cancers: Activity, chemoresistance and its overcoming. Mol Aspects Med. 2023;93:101205.
4. Kciuk M, Gielecińska A, Mujwar S, Kołat D, Kałuzińska-Kołat Ż, Celik I, et al. Doxorubicin-An Agent with Multiple Mechanisms of Anticancer Activity. Cells. 2023;12(4).
5. Brieler J, Breeden MA, Tucker J. Cardiomyopathy: An Overview. Am Fam Physician. 2017;96(10):640-6.
6. Mordente A, Meucci E, Silvestrini A, Martorana GE, Giardina B. Anthracyclines and mitochondria. Adv Exp Med Biol. 2012;942:385-419.
7. Swain SM, Whaley FS, Ewer MS. Congestive heart failure in patients treated with doxorubicin: a retrospective analysis of three trials. Cancer. 2003;97(11):2869-79.
8. Suter TM, Ewer MS. Cancer drugs and the heart: importance and management. Eur Heart J. 2013;34(15):1102-11.
9. Lipshultz SE, Lipsitz SR, Sallan SE, Dalton VM, Mone SM, Gelber RD, et al. Chronic progressive cardiac dysfunction years after doxorubicin therapy for childhood acute lymphoblastic leukemia. J Clin Oncol. 2005;23(12):2629-36.
10. Wu BB, Leung KT, Poon EN. Mitochondrial-Targeted Therapy for Doxorubicin-Induced Cardiotoxicity. Int J Mol Sci. 2022;23(3).
11. Zhang YW, Shi J, Li YJ, Wei L. Cardiomyocyte death in doxorubicin-induced cardiotoxicity. Arch Immunol Ther Exp (Warsz). 2009;57(6):435-45.
12. Carvalho FS, Burgeiro A, Garcia R, Moreno AJ, Carvalho RA, Oliveira PJ. Doxorubicin-induced cardiotoxicity: from bioenergetic failure and cell death to cardiomyopathy. Med Res Rev. 2014;34(1):106-35.
13. Songbo M, Lang H, Xinyong C, Bin X, Ping Z, Liang S. Oxidative stress injury in doxorubicin-induced cardiotoxicity. Toxicol Lett. 2019;307:41-8.
14. Gianni L, Herman EH, Lipshultz SE, Minotti G, Sarvazyan N, Sawyer DB. Anthracycline cardiotoxicity: from bench to bedside. J Clin Oncol. 2008;26(22):3777-84.
15. Ghigo A, Li M, Hirsch E. New signal transduction paradigms in anthracycline-induced cardiotoxicity. Biochim Biophys Acta. 2016;1863(7 Pt B):1916-25.
16. Kong CY, Guo Z, Song P, Zhang X, Yuan YP, Teng T, et al. Underlying the Mechanisms of Doxorubicin-Induced Acute Cardiotoxicity: Oxidative Stress and Cell Death. Int J Biol Sci. 2022;18(2):760-70.

17. Zhang S, Liu X, Bawa-Khalfe T, Lu LS, Lyu YL, Liu LF, et al. Identification of the molecular basis of doxorubicin-induced cardiotoxicity. Nat Med. 2012;18(11):1639-42.
18. Christidi E, Brunham LR. Regulated cell death pathways in doxorubicin-induced cardiotoxicity. Cell Death Dis. 2021;12(4):339.
19. Yuan J, Ofengeim D. A guide to cell death pathways. Nature Reviews Molecular Cell Biology. 2023.
20. Robertson J, Orrenius, S. Molecular Mechanisms of Apoptosis Induced by Cytotoxic Chemicals. Critical Reviews in Toxicology. 2000;30:609 - 27.
21. Cory S, Adams JM. The Bcl2 family: regulators of the cellular life-or-death switch. Nat Rev Cancer. 2002;2(9):647-56.
22. Green DR. The Mitochondrial Pathway of Apoptosis Part II: The BCL-2 Protein Family. Cold Spring Harb Perspect Biol. 2022;14(6).
23. Yuan S, Yu X, Asara JM, Heuser JE, Ludtke SJ, Akey CW. The holo-apoptosome: activation of procaspase-9 and interactions with caspase-3. Structure. 2011;19(8):1084-96.
24. Julien O, Wells JA. Caspases and their substrates. Cell Death Differ. 2017;24(8):1380-9.
25. Redza-Dutordoir M, Averill-Bates DA. Activation of apoptosis signalling pathways by reactive oxygen species. Biochim Biophys Acta. 2016;1863(12):2977-92.
26. Wajant H, Johannes FJ, Haas E, Siemienski K, Schwenzer R, Schubert G, et al. Dominant-negative FADD inhibits TNFR60-, Fas/Apo1- and TRAIL-R/Apo2-mediated cell death but not gene induction. Curr Biol. 1998;8(2):113-6.
27. Park HH. Structural features of caspase-activating complexes. Int J Mol Sci. 2012;13(4):4807-18.
28. Hansen M, Rubinsztein DC, Walker DW. Autophagy as a promoter of longevity: insights from model organisms. Nat Rev Mol Cell Biol. 2018;19(9):579-93.
29. Dikic I, Elazar Z. Mechanism and medical implications of mammalian autophagy. Nat Rev Mol Cell Biol. 2018;19(6):349-64.
30. Bartlett JJ, Trivedi PC, Pulinilkunnil T. Autophagic dysregulation in doxorubicin cardiomyopathy. J Mol Cell Cardiol. 2017;104:1-8.
31. Bartlett JJ, Trivedi PC, Yeung P, Kienesberger PC, Pulinilkunnil T. Doxorubicin impairs cardiomyocyte viability by suppressing transcription factor EB expression and disrupting autophagy. Biochem J. 2016;473(21):3769-89.
32. Li DL, Wang ZV, Ding G, Tan W, Luo X, Criollo A, et al. Doxorubicin Blocks Cardiomyocyte Autophagic Flux by Inhibiting Lysosome Acidification. Circulation. 2016;133(17):1668-87.
33. Dixon SJ, Lemberg KM, Lamprecht MR, Skouta R, Zaitsev EM, Gleason CE, et al. Ferroptosis: an iron-dependent form of nonapoptotic cell death. Cell. 2012;149(5):1060-72.
34. Ichikawa Y, Ghanefar M, Bayeva M, Wu R, Khechaduri A, Naga Prasad SV, et al. Cardiotoxicity of doxorubicin is mediated through mitochondrial iron accumulation. J Clin Invest. 2014;124(2):617-30.
35. Minotti G, Ronchi R, Salvatorelli E, Menna P, Cairo G. Doxorubicin irreversibly inactivates iron regulatory proteins 1 and 2 in cardiomyocytes: evidence for distinct metabolic pathways and implications for iron-mediated cardiotoxicity of antitumor therapy. Cancer Res. 2001;61(23):8422-8.
36. Linkermann A, Green DR. Necroptosis. N Engl J Med. 2014;370(5):455-65.
37. Yu X, Ruan Y, Huang X, Dou L, Lan M, Cui J, et al. Dexrazoxane ameliorates doxorubicin-induced cardiotoxicity by inhibiting both apoptosis and necroptosis in cardiomyocytes. Biochem Biophys Res Commun. 2020;523(1):140-6.
38. Bernuzzi F, Recalcati S, Alberghini A, Cairo G. Reactive oxygen species-independent apoptosis in doxorubicin-treated H9c2 cardiomyocytes: role for heme oxygenase-1 down-modulation. Chem Biol Interact. 2009;177(1):12-20.
39. Ambros V. The functions of animal microRNAs. Nature. 2004;431(7006):350-5.
40. Bartel DP. MicroRNAs: target recognition and regulatory functions. Cell. 2009;136(2):215-33.

41. Lee Y, Kim M, Han J, Yeom KH, Lee S, Baek SH, et al. MicroRNA genes are transcribed by RNA polymerase II. Embo j. 2004;23(20):4051-60.
42. Yi R, Qin Y, Macara IG, Cullen BR. Exportin-5 mediates the nuclear export of pre-microRNAs and short hairpin RNAs. Genes Dev. 2003;17(24):3011-6.
43. Friedman RC, Farh KK, Burge CB, Bartel DP. Most mammalian mRNAs are conserved targets of microRNAs. Genome Res. 2009;19(1):92-105.
44. Esteller M. Non-coding RNAs in human disease. Nat Rev Genet. 2011;12(12):861-74.
45. Gebert LFR, MacRae IJ. Regulation of microRNA function in animals. Nat Rev Mol Cell Biol. 2019;20(1):21-37.
46. Calin GA, Croce CM. MicroRNA signatures in human cancers. Nat Rev Cancer. 2006;6(11):857-66.
47. Greco S, Gaetano C, Martelli F. HypoxamiR regulation and function in ischemic cardiovascular diseases. Antioxid Redox Signal. 2014;21(8):1202-19.
48. Huang X, Le QT, Giaccia AJ. MiR-210--micromanager of the hypoxia pathway. Trends Mol Med. 2010;16(5):230-7.
49. Guan Y, Song X, Sun W, Wang Y, Liu B. Effect of Hypoxia-Induced MicroRNA-210 Expression on Cardiovascular Disease and the Underlying Mechanism. Oxid Med Cell Longev. 2019;2019:4727283.
50. Nallamshetty S, Chan SY, Loscalzo J. Hypoxia: a master regulator of microRNA biogenesis and activity. Free Radic Biol Med. 2013;64:20-30.
51. Gou D, Ramchandran R, Peng X, Yao L, Kang K, Sarkar J, et al. miR-210 has an antiapoptotic effect in pulmonary artery smooth muscle cells during hypoxia. Am J Physiol Lung Cell Mol Physiol. 2012;303(8):L682-91.
52. Wang F, Xiong L, Huang X, Zhao T, Wu LY, Liu ZH, et al. miR-210 suppresses BNIP3 to protect against the apoptosis of neural progenitor cells. Stem Cell Res. 2013;11(1):657-67.
53. Marwarha G, Røsand Ø, Scrimgeour N, Slagsvold KH, Høydal MA. miR-210 Regulates Apoptotic Cell Death during Cellular Hypoxia and Reoxygenation in a Diametrically Opposite Manner. Biomedicines. 2021;10(1).
54. Marwarha G, Røsand Ø, Slagsvold KH, Høydal MA. GSK3β Inhibition Is the Molecular Pivot That Underlies the Mir-210-Induced Attenuation of Intrinsic Apoptosis Cascade during Hypoxia. Int J Mol Sci. 2022;23(16).
55. Phukan S, Babu VS, Kannoji A, Hariharan R, Balaji VN. GSK3beta: role in therapeutic landscape and development of modulators. Br J Pharmacol. 2010;160(1):1-19.
56. Inoki K, Ouyang H, Zhu T, Lindvall C, Wang Y, Zhang X, et al. TSC2 integrates Wnt and energy signals via a coordinated phosphorylation by AMPK and GSK3 to regulate cell growth. Cell. 2006;126(5):955-68.
57. Lal H, Ahmad F, Woodgett J, Force T. The GSK-3 family as therapeutic target for myocardial diseases. Circ Res. 2015;116(1):138-49.
58. Beurel E, Jope RS. The paradoxical pro- and anti-apoptotic actions of GSK3 in the intrinsic and extrinsic apoptosis signaling pathways. Prog Neurobiol. 2006;79(4):173-89.
59. Wang SH, Sun MJ, Ding SY, Liu CL, Wang JM, Han SN, et al. Ticagrelor reduces doxorubicin-induced pyroptosis of rat cardiomyocytes by targeting GSK-3β/caspase-1. Front Cardiovasc Med. 2022;9:1090601.
60. Kuang Z, Wu J, Tan Y, Zhu G, Li J, Wu M. MicroRNA in the Diagnosis and Treatment of Doxorubicin-Induced Cardiotoxicity. Biomolecules. 2023;13(3).
61. Davidson MM, Nesti C, Palenzuela L, Walker WF, Hernandez E, Protas L, et al. Novel cell lines derived from adult human ventricular cardiomyocytes. J Mol Cell Cardiol. 2005;39(1):133-47.
62. Chalak M, Hesaraki M, Mirbahari SN, Yeganeh M, Abdi S, Rajabi S, et al. Cell Immortality: In Vitro Effective Techniques to Achieve and Investigate Its Applications and Challenges. Life. 2024;14(3):417.
63. Berg PC, Hansson Å ML, Røsand Ø, Marwarha G, Høydal MA. Overexpression of Neuron-Derived Orphan Receptor 1 (NOR-1) Rescues Cardiomyocytes from Cell Death and Improves Viability after Doxorubicin Induced Stress. Biomedicines. 2021;9(9).

64. Bradford MM. A rapid and sensitive method for the quantitation of microgram quantities of protein utilizing the principle of protein-dye binding. Anal Biochem. 1976;72:248-54.
65. Ghasemi M, Turnbull T, Sebastian S, Kempson I. The MTT Assay: Utility, Limitations, Pitfalls, and Interpretation in Bulk and Single-Cell Analysis. Int J Mol Sci. 2021;22(23).
66. Aydin S. A short history, principles, and types of ELISA, and our laboratory experience with peptide/protein analyses using ELISA. Peptides. 2015;72:4-15.
67. Korzeniewski C, Callewaert DM. An enzyme-release assay for natural cytotoxicity. J Immunol Methods. 1983;64(3):313-20.
68. Deverre JR, Boutet V, Boquet D, Ezan E, Grassi J, Grognet JM. A competitive enzyme hybridization assay for plasma determination of phosphodiester and phosphorothioate antisense oligonucleotides. Nucleic Acids Res. 1997;25(18):3584-9.
69. Nicholson DW, Ali A, Thornberry NA, Vaillancourt JP, Ding CK, Gallant M, et al. Identification and inhibition of the ICE/CED-3 protease necessary for mammalian apoptosis. Nature. 1995;376(6535):37-43.
70. TargetScanHuman 8.0 [Internet]. 2021 [cited 02.02.2024]. Available from: https://www.targetscan.org/vert_80/.
71. STRING 12.0 [Internet]. 2023 [cited 02.02.2024]. Available from: https://string-db.org/cgi/input?sessionId=b5GhrdLzAKDE&input_page_show_search=on.
72. Linders AN, Dias IB, López Fernández T, Tocchetti CG, Bomer N, Van der Meer P. A review of the pathophysiological mechanisms of doxorubicin-induced cardiotoxicity and aging. NPJ Aging. 2024;10(1):9.
73. Szponar J, Ciechanski E, Ostrowska-Lesko M, Gorska A, Tchorz M, Dabrowska A, et al. The Lack of Synergy between Carvedilol and the Preventive Effect of Dexrazoxane in the Model of Chronic Anthracycline-Induced Cardiomyopathy. Int J Mol Sci. 2023;24(12).
74. Kim HW, Haider HK, Jiang S, Ashraf M. Ischemic preconditioning augments survival of stem cells via miR-210 expression by targeting caspase-8-associated protein 2. J Biol Chem. 2009;284(48):33161-8.
75. Fang G, Li X, Yang F, Huang T, Qiu C, Peng K, et al. Amentoflavone mitigates doxorubicin-induced cardiotoxicity by suppressing cardiomyocyte pyroptosis and inflammation through inhibition of the STING/NLRP3 signalling pathway. Phytomedicine. 2023;117:154922.
76. Bei Y, Wang H, Liu Y, Su Z, Li X, Zhu Y, et al. Exercise-Induced miR-210 Promotes Cardiomyocyte Proliferation and Survival and Mediates Exercise-Induced Cardiac Protection against Ischemia/Reperfusion Injury. Research (Wash D C). 2024;7:0327.
77. Bian WS, Shi PX, Mi XF, Sun YY, Yang DD, Gao BF, et al. MiR-210 protects cardiomyocytes from OGD/R injury by inhibiting E2F3. Eur Rev Med Pharmacol Sci. 2018;22(3):743-9.
78. Yuan H, Zhang Q, Guo J, Zhang T, Zhao J, Li J, et al. A PGC-1α-Mediated Transcriptional Network Maintains Mitochondrial Redox and Bioenergetic Homeostasis against Doxorubicin-Induced Toxicity in Human Cardiomyocytes: Implementation of TT21C. Toxicol Sci. 2016;150(2):400-17.
79. Mutharasan RK, Nagpal V, Ichikawa Y, Ardehali H. microRNA-210 is upregulated in hypoxic cardiomyocytes through Akt- and p53-dependent pathways and exerts cytoprotective effects. Am J Physiol Heart Circ Physiol. 2011;301(4):H1519-30.
80. Shangguan H, Huang X, Lin J, Chen R. Knockdown of Kmt2d leads to growth impairment by activating the Akt/β-catenin signaling pathway. G3 (Bethesda). 2024;14(3).
81. Zhuang Y, Cheng M, Li M, Cui J, Huang J, Zhang C, et al. Small extracellular vesicles derived from hypoxic mesenchymal stem cells promote vascularized bone regeneration through the miR-210-3p/EFNA3/PI3K pathway. Acta Biomater. 2022;150:413-26.
82. Xu Y. TET2 expedites coronary heart disease by promoting microRNA-126 expression and inhibiting the E2F3-PI3K-AKT axis. Biochem Cell Biol. 2020;98(6):698-708.

83. Cui Y, Chen R, Ma L, Yang W, Chen M, Zhang Y, et al. miR-205 Expression Elevated With EDS Treatment and Induced Leydig Cell Apoptosis by Targeting RAP2B via the PI3K/AKT Signaling Pathway. Front Cell Dev Biol. 2020;8:448.
84. Zhao R, Wang X, Wang H, Yu T, Wang Q, Yang X, et al. Inhibition of long noncoding RNA BDNF-AS rescues cell death and apoptosis in hypoxia/reoxygenation damaged murine cardiomyocyte. Biochimie. 2017;138:43-9.
85. Zhao D, Zhang S, Wang X, Gao D, Liu J, Cao K, et al. ATG7 regulates hepatic Akt phosphorylation through the c-JUN/PTEN pathway in high fat diet-induced metabolic disorder. Faseb j. 2019;33(12):14296-306.
86. Xu Y, Hu T, Ding H, Yuan Y, Chen R. miR-485-5p alleviates obstructive sleep apnea syndrome with hypertension by inhibiting PI3K/AKT signaling pathway via downregulating HIF3A expression. Sleep Breath. 2023;27(1):109-19.
87. Kitakata H, Endo J, Ikura H, Moriyama H, Shirakawa K, Katsumata Y, et al. Therapeutic Targets for DOX-Induced Cardiomyopathy: Role of Apoptosis vs. Ferroptosis. Int J Mol Sci. 2022;23(3).

88. Bavelloni A, Ramazzotti G, Poli A, Piazzi M, Focaccia E, Blalock W, et al. MiRNA-210: A Current Overview. Anticancer Res. 2017;37(12):6511-21.

89. Hu S, Huang M, Li Z, Jia F, Ghosh Z, Lijkwan MA, et al. MicroRNA-210 as a novel therapy for treatment of ischemic heart disease. Circulation. 2010;122(11 Suppl):S124-31

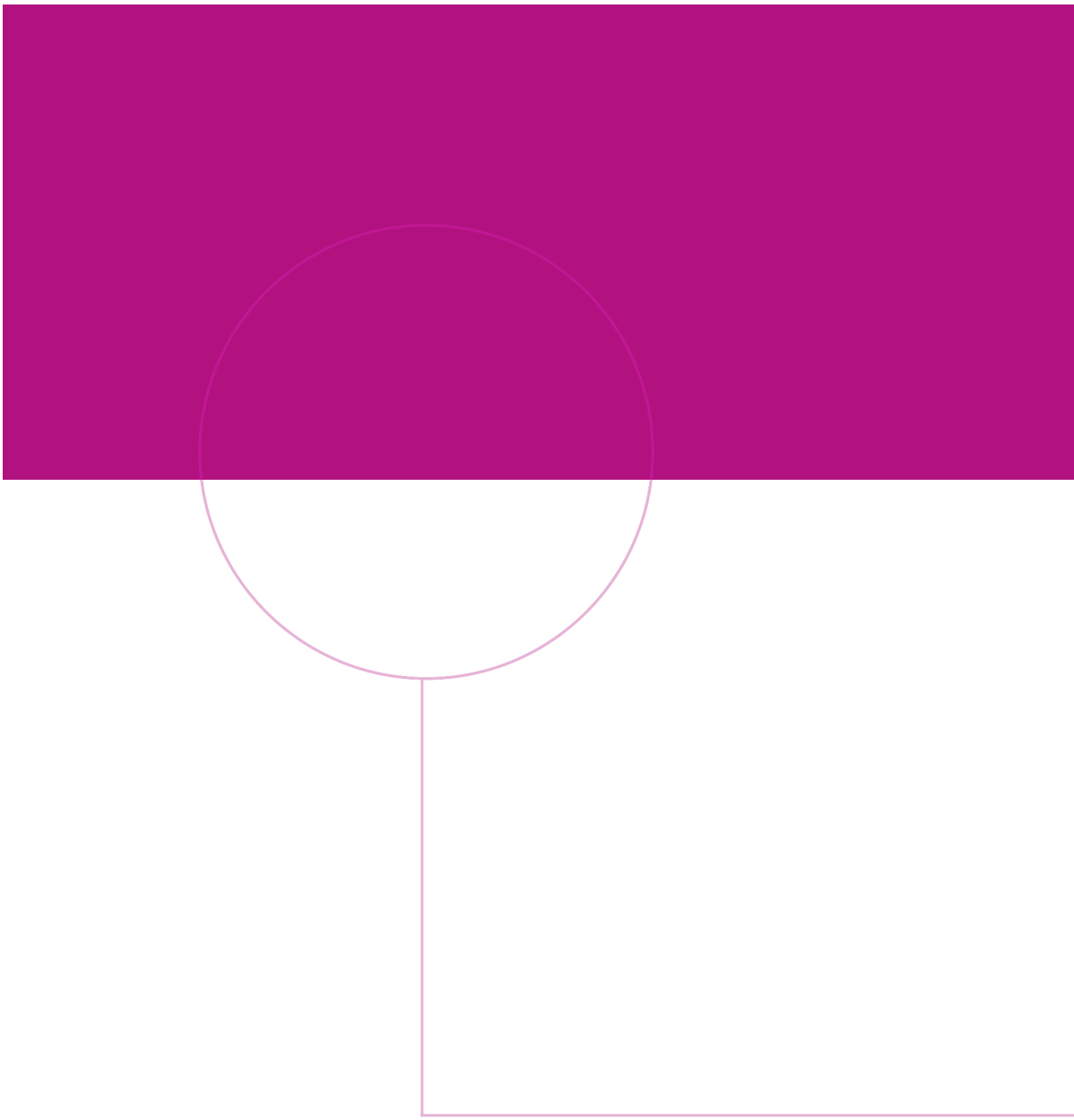

NTNU

Norwegian University of
Science and Technology